iScience

CellPress
OPEN ACCESS

Review

Recent advances in dynamic reconstruction of electrocatalysts for carbon dioxide reduction

Jianfang Zhang,[1,2] Shuai Xia,[1] Yan Wang,[1,3,*] Jingjie Wu,[2,*] and Yucheng Wu[1,4,5]

SUMMARY

Electrocatalysts undergo structural evolution under operating electrochemical CO_2 reduction reaction (CO_2RR) conditions. This dynamic reconstruction correlates with variations in CO_2RR activity, selectivity, and stability, posing challenges in catalyst design for electrochemical CO_2RR. Despite increased research on the reconstruction behavior of CO_2RR electrocatalysts, a comprehensive understanding of their dynamic structural evolution under reaction conditions is lacking. This review summarizes recent developments in the dynamic reconstruction of catalysts during the CO_2RR process, covering fundamental principles, modulation strategies, and *in situ*/operando characterizations. It aims to enhance understanding of electrocatalyst dynamic reconstruction, offering guidelines for the rational design of CO_2RR electrocatalysts.

INTRODUCTION

The continual rise in CO_2 emissions from fossil fuel consumption has unleashed severe environmental pollution and triggered alarming global climate change.[1,2] The direct conversion of CO_2 into carbon-based chemicals can help achieve carbon cycling in the environment.[3] In this regard, electrochemical CO_2 reduction reaction (CO_2RR) driven by clean and renewable electricity offers an efficient route to convert CO_2 into value-added fuels and energy-dense products.[4,5] The electrocatalytic CO_2RR process can be typically operated under ambient temperature and pressure conditions, use H_2O as the hydrogen source, and produce C_{2+} products, offering distinct advantages over technologies, such as thermocatalysis and photocatalysis.[6]

Despite notable progress in electrocatalytic CO_2RR over the past few decades, the realization of industrial applications faces numerous challenges, including limited productivity and selectivity of a specific product, low carbon efficiency due to carbon crossover, and reduced stability resulting from salt precipitates and flooding.[7–9] The productivity and selectivity of target products are intricately tied to the catalysts and reaction environment.[10–12] The catalyst dictates the reaction pathways leading to the formation of C_1 to multi-carbon (C_{2+}) products.[13] Despite numerous efforts to design highly active catalysts that enhance the activity and selectivity of CO_2RR, the dynamic structural evolution and surface reconstruction observed on various catalysts under CO_2RR conditions pose additional hurdles.[14–16] The minor changes in the catalyst structure during the reconstruction process may substantially alter the reaction pathways and reactivity of CO_2RR. It is important to note that these changes and their influencing factors are always intertwined, which complicates the discovery and design of effective catalysts. For instance, the dynamic morphology evolution of catalysts triggers surface changes to rougher or smoother, resulting in changes in phase, surface facets, and chemical states. These morphological reconstructions usually induce the alteration of local pH near the catalyst surface, which seriously affects the catalytic performance. Besides, various metal-based catalysts, particularly their oxides, undergo substantial atomic rearrangement and composition changes during reduction, leading to the reconstruction of new active sites, such as vacancy defects, grain boundaries (GBs), twin boundaries (TBs), and interfaces.[17–19] Compared with the intrinsic structure and active ingredients of the original catalysts, the regenerated active sites in the reconstructed catalysts play more important roles in the activity, selectivity, and stability of CO_2RR, and their advantages and disadvantages need to be analyzed dialectically. It should be pointed out that the dynamic structure evolution will also lead to the degradation and poisoning of the catalysts. The potential-driven reconstruction can induce structural distortion and collapse, chemical components change, and agglomeration or dissolution, leading to the deactivation of the catalysts.[20–22] The in-depth understanding of catalyst degradation under dynamic evolution is expected to provide guidance for enhancing the stability of CO_2RR.

Therefore, unveiling the genuine active sites of reconstructed catalysts becomes crucial for understanding the reaction mechanism of CO_2RR.[23,24] Advanced *in situ*/operando techniques have been explored in recent years to investigate the dynamic reconstruction behavior of catalysts and correlate them with real-time CO_2RR activity and selectivity.[25–28] For example, the employment of *in situ* electrochemical microscopy techniques such as scanning tunneling microscopy (STM), atomic force microscopy (AFM), scanning electron microscopy (SEM), and

[1]School of Materials Science and Engineering, Hefei University of Technology, Hefei 230009, China
[2]Department of Chemical and Environmental Engineering, University of Cincinnati, Cincinnati, OH 45221, USA
[3]Institute of Energy, Hefei Comprehensive National Science Center (Anhui Energy Laboratory), Hefei 230009, China
[4]Key Laboratory of Advanced Functional Materials and Devices of Anhui Province, Hefei University of Technology, Hefei 230009, China
[5]China International S&T Cooperation Base for Advanced Energy and Environmental Materials & Anhui Provincial International S&T Cooperation Base for Advanced Energy Materials, Hefei University of Technology, Hefei 230009, China
*Correspondence: stone@hfut.edu.cn (Y.W.), wu2jj@ucmail.uc.edu (J.W.)
https://doi.org/10.1016/j.isci.2024.110005

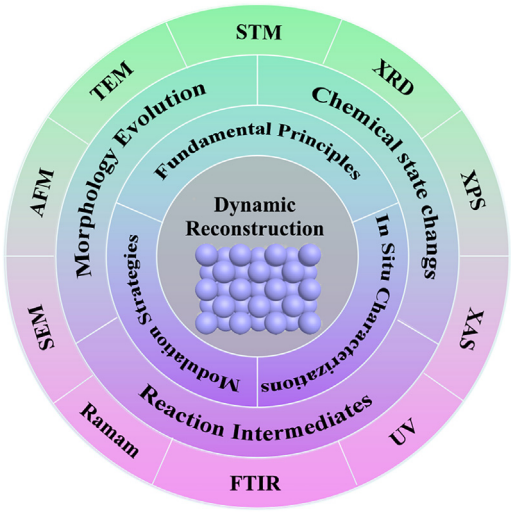

Figure 1. Overview of major topics discussed in this review.

transmission electron microscopy (TEM) can reveal the dynamic morphological evolution of catalysts under reaction conditions. Operando X-ray diffraction (XRD) and X-ray absorption spectroscopy (XAS) provide direct evidence for the transformation of phase structure and composition of reconstructed catalysts. Moreover, the chemical state and active species on the catalyst surface can be detected by quasi-*in situ* X-ray photoelectron spectroscopy (XPS) and *in situ* Raman spectroscopy. Besides, *in situ*/operando spectroscopy, such as Raman, Fourier transform infrared (FTIR), and UV-Vis adsorption spectra, probes the adsorbed species on the catalyst surface with characteristic peaks/bands. Monitoring the adsorbed reaction intermediates contributes to disclosing the reconstruction behavior of the catalysts during the catalytic reaction as the adsorption configuration is sensitive to surface active sites. More importantly, when combined with density functional theory (DFT) computations, these techniques can shed light on the structure-property relationship of reconstructed catalysts, providing a deep understanding of the reaction mechanism based on the adsorption of reaction intermediates on the active sites.[29–31] The previous work has reviewed the dynamic reconstruction with a focus on the changes of the catalyst structure and the reaction environments during CO_2RR.[32] However, due to the rapid development of catalysts and catalytic technologies for CO_2RR, it is necessary to timely review the latest advances in dynamic catalysis, new catalytic processes and modulation strategies to control dynamics, and *in-situ*/operando techniques to track the dynamics.

Herein, we present an overview of recent advances in the dynamic reconstruction of CO_2RR electrocatalysts, placing special emphasis on fundamentals of reconstruction behavior, modulation strategies for catalyst surface evolution, and *in situ*/operando techniques for monitoring reconstruction processes (summarized in Figure 1). Firstly, we provide a concise examination of fundamental principles of dynamic reconstruction, encompassing thermodynamics, and kinetics aspects. Following that, we systemically outline typical strategies for modulating catalyst surface evolution, covering the regulation of catalyst composition, electrolyte type and catalytic process (e.g., pulsed electrolysis). Thirdly, several *in situ*/operando techniques are introduced to track the reconstructing process, including structural characterizations, chemical states analysis, and reaction intermediates detection. Finally, we critically assess future opportunities and challenges pertaining to catalyst reconstruction in electrocatalytic reactions, summarizing potential advancements, and prospecting forthcoming developments. This review aims to advance understanding of the dynamic reconstruction of catalysts in CO_2RR, inspiring the catalyst design to meet the requirements of productivity and selectivity toward a single product.

FUNDAMENTAL UNDERSTANDING OF DYNAMIC RECONSTRUCTION

The dynamic evolutions of the catalysts have been widely observed during the CO_2RR process. In general, the dynamic reconstruction process under CO_2RR conditions usually causes multiple changes of the catalysts, including the phase, chemical state, and morphology (facet, shape, and size) (Figure 2). The atomic migration in the reconstructed catalysts often results in highly active sites such as interfaces (e.g., homo- or heterojunction, terrace, step), and defects (e.g., grain boundary or twin boundary, pore or vacancy, doping).[33] Understanding the reconstruction behavior of the catalysts are crucial for elucidating the source of catalytic activity and selectivity. In this section, we focus on the fundamentals of electrochemical reconstruction behaviors in terms of thermodynamic and kinetic and the classification of the reconstruction mechanisms.

Redox transformation

The catalysts potentially undergo redox transformation involving phase transition and chemical state evolution under CO_2RR conditions. The connection between thermodynamic and kinetic behavior is essential to trace the origin of dynamic reconstruction.[34] From a thermodynamic perspective, the phase transition of a metal-based catalyst hinges on its standard redox potentials.[35] Referencing the well-known Pourbaix diagram, the stable phase of an element is contingent on pH and potentials in the aqueous electrochemical system. Generally, the oxidation

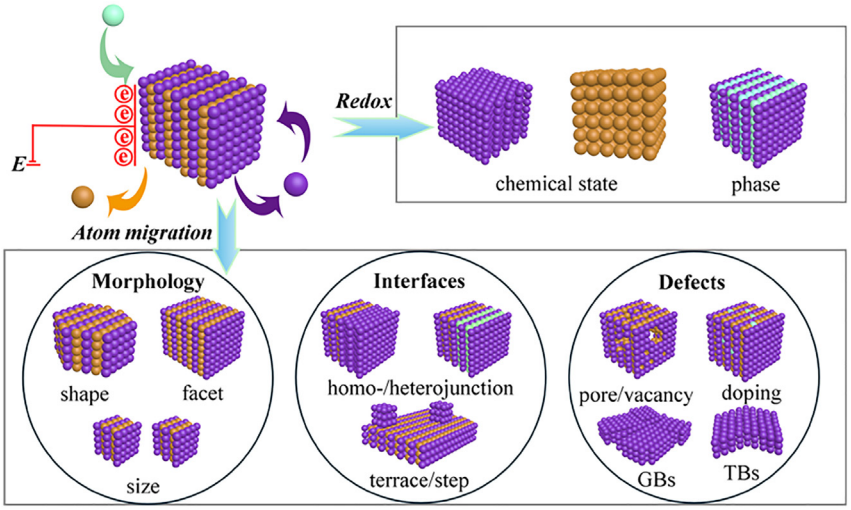

Figure 2. Summary of catalyst reconstruction behavior.

state of metal elements occupies a relatively positive potential region, transitioning into a metallic state at more negative potentials. The pH value complicates matters by influencing the oxidation species and dissolution of the metal element. The Pourbaix diagram suggests that metal oxides can supposedly undergo spontaneous reduction at cathodic potentials, forming thermodynamically stable metallic phases under CO_2RR conditions. Yet, the intricacies and potential pitfalls associated with these thermodynamic considerations must be critically evaluated.

The apparently comprehensive Pourbaix diagram, although widely referenced, tends to oversimplify the complex reality of metal-based catalysts under CO_2RR conditions. Contradictory experimental results frequently emerge, highlighting the idealized diagram's limitations that fail to account for various influencing factors. Therefore, to address the discrepancies and constraints of the Pourbaix diagram, the kinetics behavior must be considered.[34,35] The reduction of metal oxide invariably alters the chemical state of metal elements, often resulting in the removal of oxygen from the catalysts. However, the depletion of oxygen anions from the surface to the catalyst's interior becomes challenging, introducing obstacles to total oxygen removal due to energy barriers associated with migration. Consequently, from a kinetics perspective, the thermodynamically unstable oxidation phase persists on a cathodic basis. Adding to the intricacies, the reconstruction process occurs under a broad spectrum of reaction conditions, such as electrolyte, temperature, and reaction microenvironment, resulting in different phases and surface oxidation states.[36–38] These structural evolutions contribute to a heightened kinetic barrier for oxygen removal, further aiding in the stabilization of the oxidation state within the catalyst.

Atomic migration

Atomic migration induces atomic rearrangement accompanied by size, facet, and atomic distribution alterations. The initial consideration in analyzing atomic rearrangement or migration involves thermodynamic propriety, where changes in Gibbs free energy (ΔG_{am}) can be expressed as follows:

$$\Delta G_{am} = \Delta H_{am} - T\Delta S_{am} + \Delta\gamma_{am}A$$

Where ΔH_{am}, ΔS_{am}, and $\Delta\gamma_{am}$ represent the enthalpy, entropy, and specific surface energy differences before and after atomic migration, respectively. T denotes the absolute temperature, and A is the surface area of the catalyst.[39,40] Atomic migration is more likely to occur in systems with a more negative ΔG_{am}. The structure characteristics, including composition, size, and shape, of catalysts with different atomic bonding strengths and surface energies play a pivotal role in determining the favorability of atomic migration. Diverse vacancy formation energy arising from varying atomic bonding strengths of metals leads to distinct trends in reconstruction under CO_2RR conditions. In addition to single metals, the presence of multiple components in metal alloys introduces complexity to the atomic arrangement, complicating element redistribution during atomic migration. The reconstruction behavior is also associated with the morphological structure of catalysts. According to the perspective of Ostwald ripening, size-dependence surface energy induces the solubility difference, resulting in substance migration and size changes in nanoparticles.[41] Small particles are initially dissolved into the electrolyte to reduce system energy, followed by the re-deposition of dissolved atoms onto larger particles. Furthermore, the shape of the catalysts typically undergoes evolution with the reconstruction of the surface facet and redistribution of coordinated atoms.[20] Concerning rearrangement, the atomic migration process is inclined to form thermodynamic stable surfaces. In particular, atomic migration is more likely to occur on high-index facets due to more unstable and undercoordinated sites.[42]

The study of atomic migration behavior can also be approached through kinetic characteristics, as described by the Arrhenius equation:

$$k_{am} = k_0 \exp(-E_{am} / RT)$$

where k_{am}, k_0, and E_{am} are the migration rate constant, preexponential factor, and atomic migration energy barrier, respectively.[43] Clearly, the value of k_{am} or the rate of atomic arrangement heavily relies on the migration barrier (E_{am}). The intrinsic properties of the catalysts exert a substantial influence on E_{am}, in the context of single metal atoms or alloy atoms.[44,45] The exposed surface facets contribute to different E_{am}, exemplified by the Pd (110) surface with the highest E_{am} preventing atomic detachment from the catalyst surface.[46] Beyond catalyst structure, the presence of reaction intermediates such as *H and *CO adsorbed on the catalyst surface can alter the E_{am} of surface atoms.[47] The surface adsorption of CO_2RR intermediates decreases the E_{am} and facilitates the atomic evacuation from the catalyst surface.[48] Moreover, the reaction environment conditions also impact the catalysts' atomic migration. According to the Arrhenius equation, the value of k_{am} can be modulated by the reaction temperature. Increasing the reaction temperature enhances the atomic vibration near the equilibrium position, enabling the crossing of the migration barrier.[49] The applied electrical field, by contrast, holds great potential to drive atomic migration in specific directions.[50] The electric field on the catalyst surface or at the electrode-electrolyte interfaces can trigger structural transformations such as surface roughening, size changes, and grain evolution.[46] The electrolyte also plays a crucial role in the dynamic evolution of catalysts, regulating the activity and selectivity of CO_2RR.[51,52] The proton depletion at the cathode surface in the CO_2RR process causes the pH changes along with the distance from the electrode to the electrolyte.[9,53,54] The dynamic variation of local pH alters the surface energy between the electrolyte and catalyst surface, leading to the structural evolution of the catalyst. Additionally, the type and concentration of the cations and anions in the electrolyte affect the activity and stability of catalysts.[55,56] The specific adsorption of anions (such as halide ions) can induce the electrochemical reconstruction of the catalyst.[57,58] Moreover, additives in the electrolyte may stabilize the surface oxidation state of the catalyst, in return driving the structural evolution under CO_2RR conditions.[59]

It should be emphasized that atomic migration is closely linked with the redox transformation. During redox reactions, metal ions can be triggered to leach from the pre-catalyst surface into the electrolyte, where they are subsequently reduced to metal atoms and redeposited on the electrode under cathodic voltage conditions. Additionally, oxygen desorption from metal oxides creates vacancies in the lattice, facilitating atomic diffusion, reducing system energy, and inducing structural reconstruction of the catalysts. Therefore, the phase transition and chemical state evolution are often accompanied by atomic rearrangement with structural evolution in morphology (size, shape, facet), interfaces, and defects. These general phenomena can be observed in the metal/metal oxides and heteroatom-incorporated metal compounds, which will be discussed in detail in section 3.

Catalyst classification

Cu-based catalysts

Since Cu-based catalysts are favorable for the conversion of CO_2 to C_{2+} products, their structural evolution has received extensive attention.[60–62] The relevant works mainly focus on understanding the dynamic structural evolution of Cu-based catalysts, including redox-induced chemical state and phase transitions, as well as atomic migration in morphology, interfaces, and defects. Yang's group revealed the structural evolution of Cu nanoparticles into active Cu nanograins during CO_2 reduction through operando electrochemical scanning transmission electron microscopy (EC-STEM) studies.[14] Taking 7 nm Cu nanoparticles as an example, parts of nanoparticles were already aggregated after the linear sweep voltammetry (LSV) scan from 0.4 to 0 V. The aggregated nanoparticles were further grown into Cu nanograins with a size of 50–100 nm after the initial state of electroreduction at 0 V. When exposed to air, O atoms were inserted into tetrahedral sites of the Cu lattice in small Cu nanoparticles, evolving into Cu_2O nanocubes. The transformation of the polycrystalline Cu surface to Cu (111) and Cu (100) facets was observed under the surface reconstruction process during CO_2 reduction, which could reasonably explain the selectivity of the CO_2RR product.[60] The adsorption of H or CO intermediates was considered to be the driving force for the restructuring of Cu surfaces.[61,63] The changes in shape and size have also been widely reflected in the morphology evolution of Cu catalysts. Recent advancements in understanding catalyst surface evolution involving *in-situ* electron microscopy experiments shed light on reconstruction behavior. For instance, electrochemical transmission electron microscopy (EC-TEM) measurements have depicted Cu_2O cube fragmentation and redeposition into nanoparticles (Figure 3A).[64] Additionally, a potential-driven nano-clustering phenomenon of differently sized Cu nanocubes has been associated with the degradation mechanism observed in metallic catalysts during electrochemical CO_2RR (Figure 3B).[65] These investigations also underscored the critical relationship between the product selectivity of CO_2RR and the initial size of catalysts.

The alteration in the chemical state inevitably accompanies the structure change during the dynamic reconstruction process, leading to the creation of more active defective sites and interfaces.[66–68] Typical reconstruction process can be observed on Cu compounds such as oxides, sulfides, halides, phosphides, etc. These reconstructed Cu catalysts offered potential promising for enhancing CO_2 reduction to C_{2+} products. The reconstruction process tends to trigger the *in-situ* generation of the Cu^+/Cu^0 interface, deemed a high catalytic site for CO_2RR. This interface in oxide-derived Cu catalyst provides adjacent Cu^+ and Cu^0 surface sites suitable for *CO adsorption in two different configurations of atop-bound *CO (CO_{atop}) and bridge-bound *CO (CO_{bridge}).[69,70] The enhanced adsorption of *CO at Cu^+ and Cu^0 sites ensures a high *CO coverage for CO dimerization, favoring the kinetics of CO_2RR to C_{2+} products.[71,72] Nonetheless, achieving a stable Cu^+/Cu^0 interface on Cu catalysts remains challenging due to the rapid reduction of Cu^+ species under CO_2RR conditions. Our recent research has revealed that GB-rich Cu nanosheets derived from CuO nanosheets possess numerous low-coordinated Cu atoms across GBs.[73] These low-coordinated Cu cluster atoms have a more negative electrochemical standard reduction potential than bulk metal, maintaining the oxidation state to form stable Cu^+/Cu^0 interfaces during CO_2RR (Figures 3C–3E). Compared to Cu GBs and Cu_2O GBs, these reconstructed Cu^+/Cu^0 interfaces

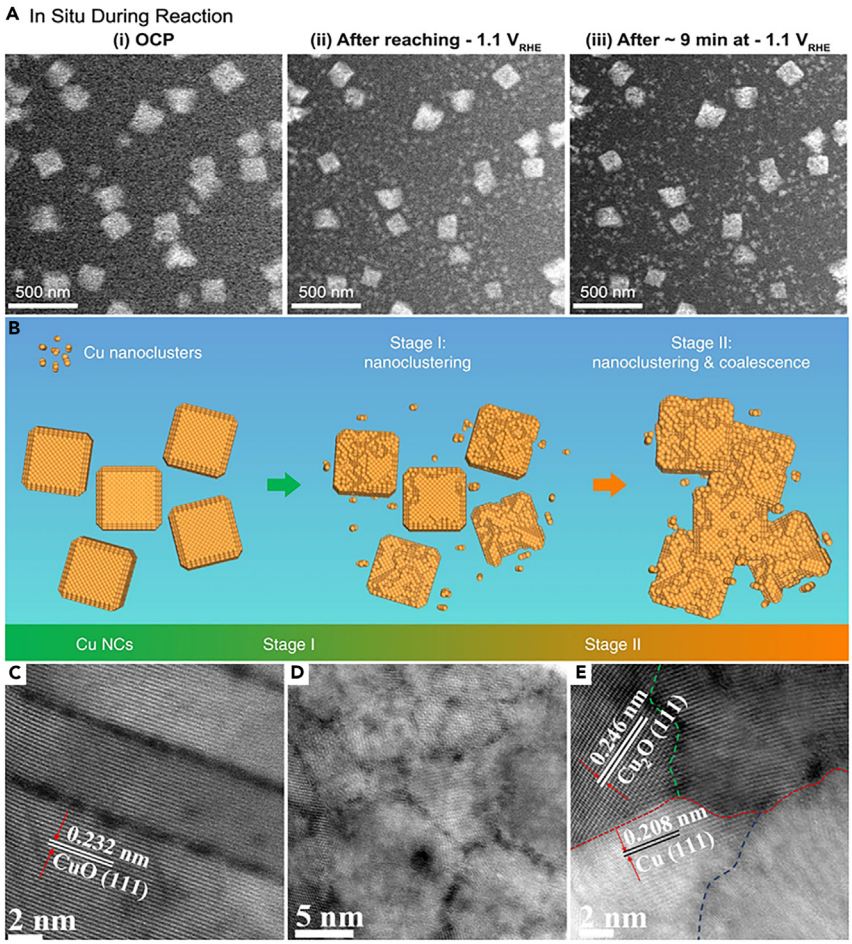

Figure 3. Structural evolution of Cu-based catalysts

(A) Morphology evolution of Cu_2O cubes during CO_2RR. Reproduced with permission.[64] Copyright 2021, Springer Nature.

(B) Schematic illustration of the degradation of Cu nanocubes during CO_2RR. Reproduced with permission.[65] Copyright 2018, Springer Nature.

(C–E) *Ex situ* STEM image of CuO nanosheets (C) before and (D and E) after CO_2RR. Reproduced with permission.[73] Copyright 2022, Wiley-VCH.

are more conducive to the formation of *CO intermediates and promote the *CO dimerization to C_2H_4 with a 62.5% FE and a partial current density of 173 mA cm^{-2} at a potential as low as −0.52 V vs. reversible hydrogen electrode (RHE, thereafter). The $Cu_{2-x}S$ derived Cu nanoparticles exhibited high performance of C_2H_4 production through a *COCHO pathway.[67] The desulphurization and surface reconstruction process contributed to creating rich high-index facets, which acted as surface active sites for the C-C coupling. The anodic halogenation of Cu followed by electroreduction could create a high density of defect sites with relatively low roughness, which promoted the adsorption of carbon intermediates and facilitated C-C coupling to C_{2+} products.[74]

Furthermore, the surface reconstruction of pre-catalysts with different morphologies often exposes specific crystal facets, significantly influencing the catalytic performance of CO_2RR. Notably, selective exposure of Cu (100) facets promotes CO dimerization toward C_{2+} products with C_2H_4 as the dominant product. For example, various morphology-dependent Cu_2O pre-catalysts were reduced to Cu catalysts with distinct ratios of crystal planes.[75] The prevalence of Cu (100) facets in the Cu nanosheet catalyst facilitated CO adsorption, resulting in increased *CO surface coverage, thereby exhibiting superior selectivity of CO_2RR toward C_{2+} products compared to Cu (110) and (111) facets.

Other metal-based catalysts

In addition to Cu-based catalysts, non-Cu metal catalysts such as Ag, Au, Pd, Bi, Sn, In, and Zn are also widely used for catalyzing CO_2 reduction. In general, CO and formate are the major products of these catalysts. The hydrogenation of *CO intermediate to CH_4 can also be achieved by regulating their electronic structures. However, the activity and selectivity of C_{2+} products of these catalysts are still severely limited. When compared with Cu catalysts, noble metals exhibit relatively inert activity due to higher vacancy formation energy or atomic migration barriers in the lattice. As a result, noble metals undergo moderate structural evolution under typical reaction conditions. Nonetheless, some relevant dynamic structural evolutions in morphology, facet, phase, and chemical state have always occurred on Pd, Au, and Ag

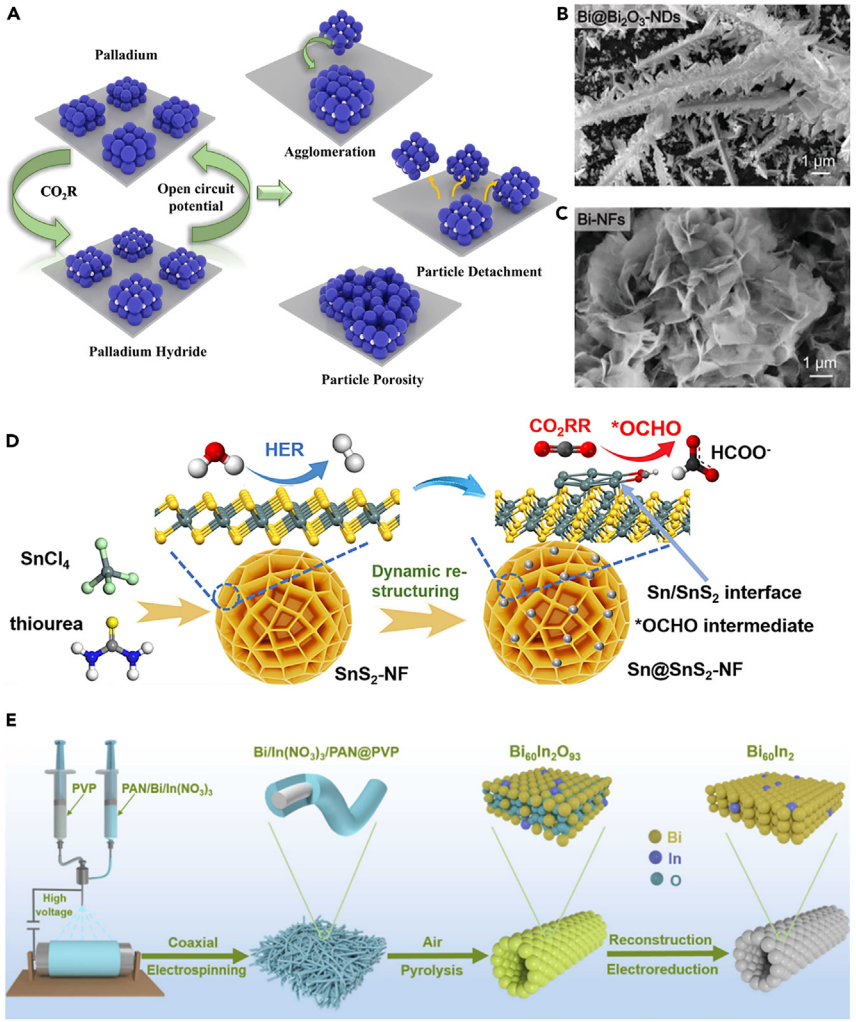

Figure 4. Reconstruction of other metal-based catalysts

(A) Schematic depiction of the morphological evolution of Pd/PdH_x catalysts. Reproduced with permission.[78] Copyright 2024, Springer Nature. SEM images of (B) Bi@Bi_2O_3 nanodendrites and (C) Bi nanoflowers. Reproduced with permission.[81] Copyright 2023, Wiley-VCH.

(D) Schematic illustration of synthetic procedure and restructuring of the SnS_2 nanoflowers. Reproduced with permission.[82] Copyright 2024, Elsevier.

(E) Schematic illustration of the preparation process for $Bi_{60}In_2$ nanotube. Reproduced with permission.[84] Copyright 2024, Elsevier.

catalysts. The defect-rich ultrathin hexagonal Pd nanosheets with dominant (111) facets were transferred to irregularly crumpled structures with active (100) sites under a dramatic surface reconstruction process during CO_2RR. The increase of active sites and the decrease of CO binding strength on Pd surfaces promoted the selectivity of CO_2 conversion to CO with FE up to 93%.[76] The phase transition of Pd to PdH_x phase was observed as a function of electrode potential under CO_2RR conditions. The formation of a hydrogen-adsorbed Pd surface on the mixture of the α- and β-phases of the PdH_x core above −0.2 V was conducive to the formation of formate, whereas the formation of a metallic Pd surface on a β-phase PdH_x core below −0.5 V promoted CO production.[77] A recent study revealed a similar evolution of Pd/PdH_x catalyst, involving morphology change and phase transformation (Figure 4A). The switchable product selectivity from formate to CO/H_2 was attributed to potential-dependent reaction energetic changes rather than the PdH_x lattice expansion.[78] Vertical standing Ag nanosheet shells were grown on the outer surface of Ag hollow fiber by an electrochemical surface reconstruction approach, which achieved a high FE of CO_2 to CO over 97% at a current density of 2.0 A cm^{-2}.[79]

As for the main group p-block metals, such as Bi, Sn, and In, structural evolution occurs frequently under a potential-driven reconstruction process. Similar to Cu, the metallic phase derived from the electroreduction of their compounds acted as the real active site for CO_2RR. The *in situ* reconstruction of $Bi(OH)_3$ nanosheets into Bi nanosheets resulted in forming a large number of coordinatively unsaturated sites, which was favorable to stabilize the *OCHO intermediates and facilitate the reaction kinetics for the formate production.[80] The Bi@Bi_2O_3 nanodendrites were reconstructed to Bi nanoflower through *in situ* electroreduction in $KHCO_3$ solution (Figures 4B and 4C). By maximizing the exposed active sites and Bi^0 species, the resultant Bi nanoflower exhibited high selectivity to the formate production with an FE of 92.3% at −0.9

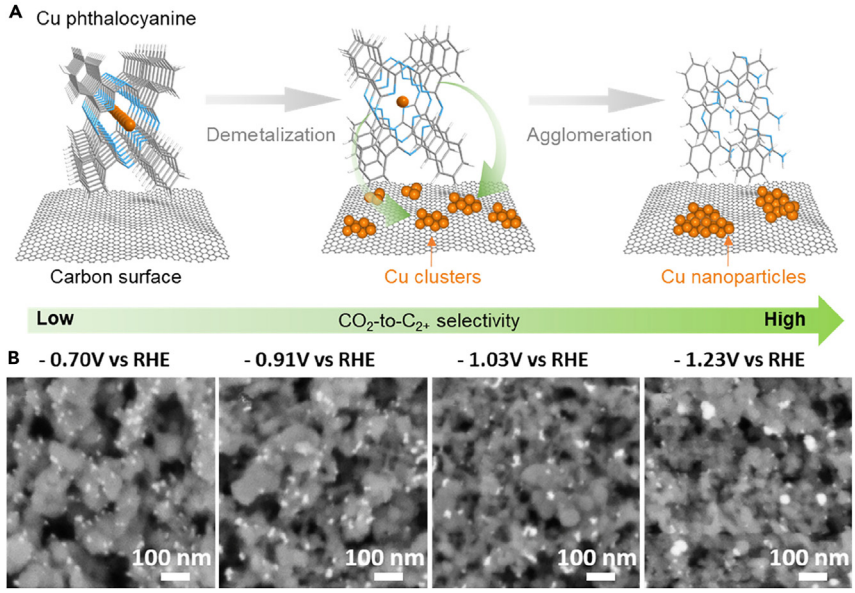

Figure 5. Evolution of molecular and single-atom catalysts

(A) The schematic of structural evolution process of CuPc and (B) backscattered electron images of CuPc catalyst after 13 min of CO_2RR at various potentials in 0.1M $KHCO_3$. Reproduced with permission.[86] Copyright 2023, American Chemical Society.

V.[81] The dynamic structural evolution of SnS_2 nanoflowers under CO_2RR conditions led to the formation of Sn nanocluster on SnS_2 substrate (Figure 4D). The interfacial boundary between the Sn nanocluster and SnS_2 substrate promoted the hydrogenation of CO_2 to *OCHO intermediate instead of the dissociation of H_2O to *H, resulting in high selectivity of formate production.[82] Similarly, *in situ* electrochemical reduction of In_2O_3 enabled the formation of In/In_2O_3 heterointerface with stable In-O species, which could regulate the electronic structure of the electrode and accelerate the protonation of CO_2RR intermediates, thereby improving the electrocatalytic performance.[83] The construction of a bimetallic interface or doped heteroatom is also an effective way to regulate the electronic structure of catalysts. A hollow-structured $Bi_{60}In_2$ nanotube was obtained by *in situ* restructuring the $Bi_{60}In_2O_{93}$ precursor under CO_2RR conditions (Figure 4E). Benefiting from the In-doping modulated electronic structure and hollow nanotube structure, the reconstructed $Bi_{60}In_2$ catalyst achieved an ampere-level current density for formate production.[84] In addition, the metal Zn was considered to be the active catalyst for CO_2RR to produce CO. For instance, the oxygen-derived Zn catalyst from the reconstruction of ZnO precursor exhibited great potential for reduction of CO_2 to CO with high activity, selectivity, and stability.[85]

Molecular and single-atom catalysts

Molecular catalysts with various ligands and metal centers are used for CO_2RR due to their unique structure, electronic, and catalytic properties. The predominantly metal centers (Cu, Fe, Ni, Bi, In, etc.) were coordinated with ligands such as porphine, polymer, and phthalocyanine. These molecular catalysts are usually unstable and tend to undergo reconstruction under CO_2RR conditions. A dynamic evolution of Cu phthalocyanine (CuPc) was observed during CO_2RR with successive procedures from the demetallation of CuPc to Cu atoms followed by the agglomeration of Cu atoms to Cu clusters and finally Cu nanoparticles (Figures 5A and 5B). The CuPc-derived Cu nanoparticles with exposure of rich GBs showed a maximum FE of 70% for C_{2+} products with a high current density of 800 mA cm^{-2} at −0.73 V[86] The indium coordination polymer precursor was transformed to indium nanosheets (In-NSs) through the electrochemical reconstruction process, which exhibited a high FE of 96.3% for formate production with a partial current density exceeding 360 mA cm^{-2} and a long-term stability for 140 h with negligible degradation.[87] Moreover, metal-organic frameworks (MOFs) and covalent organic frameworks (COFs) are typical molecular catalysts with multiple coordination centers in organic frameworks. The electrochemical reconstruction of MOFs or COFs precursors can produce highly active metal sites for CO_2RR. For example, the Cu/Cu_2O nanoclusters were prepared by *in situ* electrochemical reconstruction of Cu-N coordinated MOFs precursor, which achieved an FE of 70% toward C_2H_4 synthesis.[88] The Bi-MOFs derived Bi-based catalysts introduced unsaturated surface Bi atoms sites for highly active and selective formate production.[89,90] Atomically dispersed Co^{2+} was grafted in a redox-active COF for the selective electroreduction of CO_2 to ethanol. The oxidation state and coordination environment of a single Co site undertaken transiently changes during the CO_2RR process.[91]

In addition, atomically dispersed single-atom catalysts are often dynamically reconstructed under the driven force of potential to form clusters or nanoparticle catalysts. The potential-dependent transformation between the single atom and the clusters was reported reversible. Taking the atomic Cu catalyst as an example, Xu et al. revealed that the carbon-supported dispersed Cu atoms were reconstructed into Cu_n clusters (n = 3 and 4) with a reversible transformation under the CO_2RR conditions. Cu_n clusters achieved a record selectivity of CO_2 to ethanol

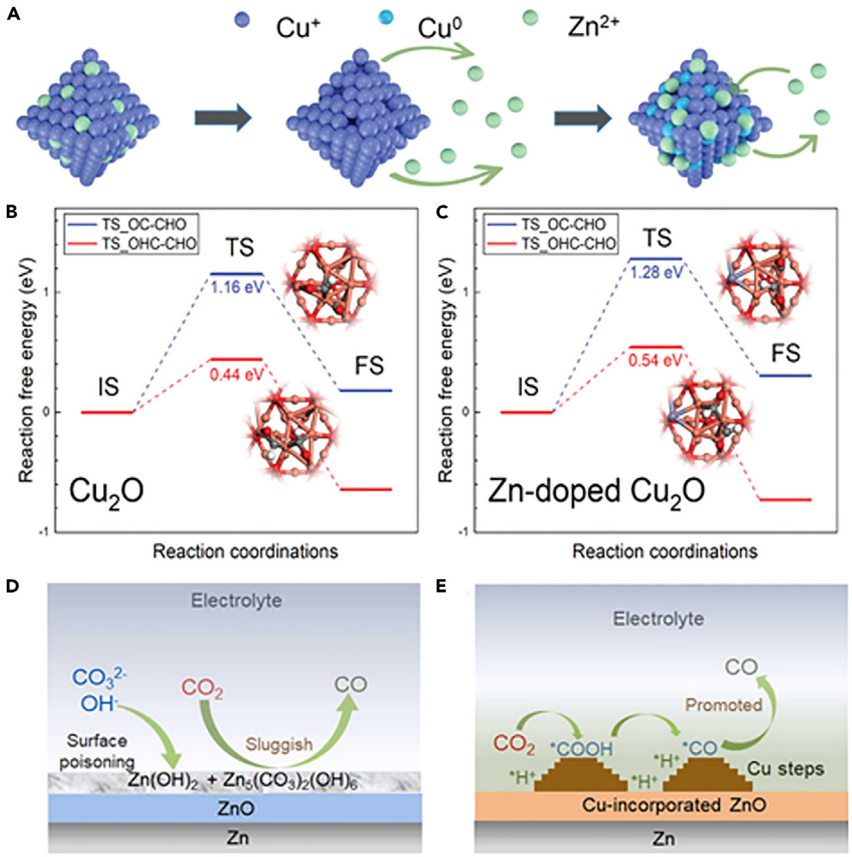

Figure 6. Incorporation of metal heteroatoms into catalysts

(A) Scheme for dissolution and redeposition mechanism of Cu_2O–Zn catalysts under CO_2RR.

(B and C) Activation barrier diagram of C–C coupling via OC–CHO and OHC–CHO pathways on (B) Cu_2O and (C) Zn-doped Cu_2O. Reproduced with permission.[95] Copyright 2023, Wiley-VCH.

(D and E) Scheme of CO_2RR mechanism on (d) ZnO and (E) Cu-incorporated ZnO surface. Reproduced with permission.[96] Copyright 2023, Elsevier.

conversion with a high FE of 91% at −0.7 V in an H-cell.[92] Their further research uncovered the relationship between the active site structure and properties of these atomically Cu catalysts. Comprehensive structural analysis revealed that the Cu atoms first aggregated to form Cu_n clusters or nanoparticles under the reduction condition, and then decomposed into smaller oxidized clusters after electrolysis. The activity and selectivity of CO_2RR were related to the size of the reconstructed Cu_n clusters or nanoparticles. Small-size Cu_n clusters (n = 3∼6) were more active for CO and ethanol formation, while large Cu_n particles (n > 55) were responsible for CH_4 and formate production.[93] The change of morphology and structure of a single-atom catalyst can adjust the adsorption and electron transfer properties of the catalyst, so as to change the reaction pathways. Tracking the dynamic evolution process of reconstructing single-atom catalysts is crucial to uncovering the reaction mechanism of CO_2RR, which requires advanced *in situ*/operando characterization techniques such as electron microscopes and spectroscopy techniques.

MODULATION STRATEGIES FOR SURFACE RECONSTRUCTION

The structural evolution of the catalysts is a common phenomenon in electrocatalysis and plays an important role in regulating catalytic activity, selectivity, and stability. The construction of high-performance electrocatalysts by rational reconstruction process has become a hot research topic in the field of electrocatalysis. Accordingly, we discuss some modulation strategies for surface reconstruction in this section, including heteroatom incorporation, electrolyte effect, pulsed electrolysis, and so on.

Heteroatom incorporation

The incorporation of metal heteroatoms into catalyst lattices commonly initiates surface reconstruction under electrocatalytic reaction conditions. This metal doping-induced surface reconstruction yields highly active components and modulates the electronic structure of metal-based catalysts.[94] For instance, in the case of Zn-doped Cu_2O nano-octahedrons catalyst, surface reconstruction occurs through leaching and redeposition of Zn during CO_2RR, creating abundant Cu-Zn bimetallic sites at the surface (Figure 6A). This Zn doping also increases the

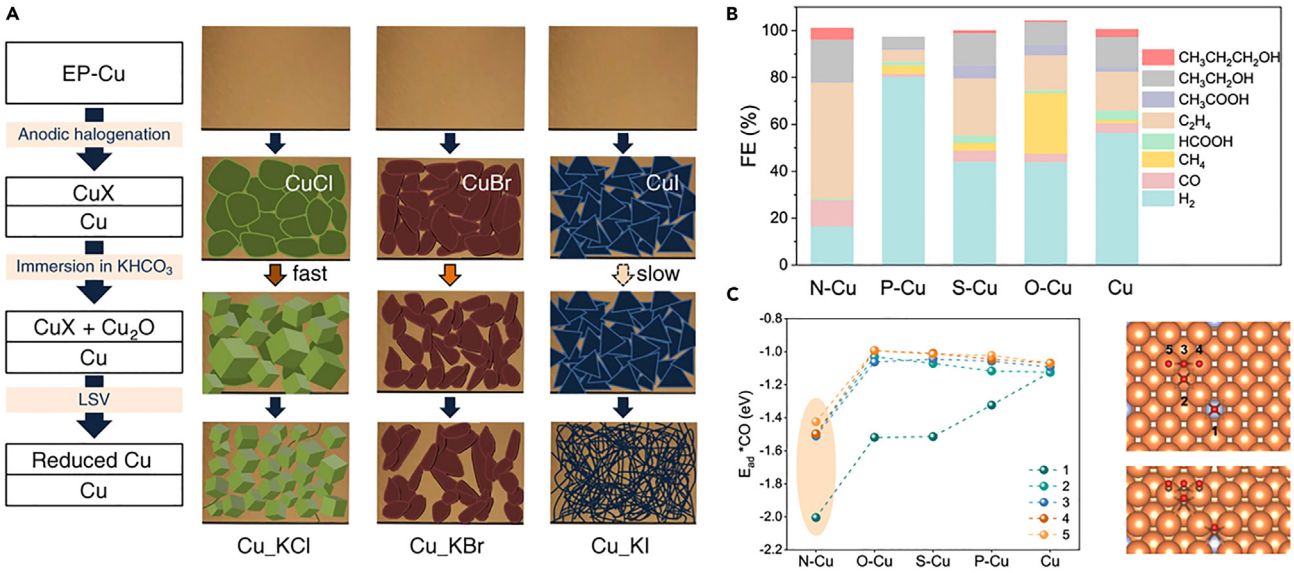

Figure 7. Incorporation of non-metal heteroatoms into catalysts

(A) Preparation process of reduced Cu catalysts. Reproduced with permission.[74] Copyright 2020, Springer Nature.

(B) Product distribution of X-Cu at −1100 mA cm^{-2}.

(C) Adsorption energy of *CO at various sites on X-Cu and Cu (100) surfaces. Reproduced with permission.[110] Copyright 2022, American Chemical Society.

percentage of Cu^0 species on the surface of the reconstructed Cu_2O-Zn catalyst, consequently leading to the formation of more Cu^0/Cu^+ interface. Benefiting from the Cu-Zn bimetallic site and Cu^0/Cu^+ interface, the introduction of Zn to Cu_2O promotes the C_2H_4 formation through the OHC-CHO pathway rather than the OC-CO and OC-CHO pathways (Figures 6B and 6C).[95] Another example involves Cu-incorporated ZnO. A metallic phase is *in situ* generated on the surface, which prevents the formation of $Zn_5(CO_3)_2(OH)_6$ and $Zn(OH)_2$ components during the CO_2RR process.[96] The segregation of Cu ions on the surface leads to the formation of stepped Cu sites in the reconstruction process (Figures 6D and 6E). These reconstructed Cu steps improve reactant adsorption/activation and intermediate stabilization, thus promoting the conversion of CO_2 to CO. The leaching of S elements from CuS-Bi_2S_3 heterojunction precursor during CO_2RR results in the formation of Cu-doped Bi catalyst. An electron-rich surface of Cu-doped Bi can be formed by upshifting the Fermi level, which is beneficial to the electron injection of CO_2 to generate CO_2^{*-} intermediate and then promote the formation of *OCHO.[23] The resultant Cu-doped Bi catalyst achieved an industrial-compatible current density of 1.1 A cm^{-2} and a high formate formation rate of 21.0 mmol h^{-1} cm^{-2} at −0.86 V in a flow cell. More importantly, it also realized over 90% FE and superior long-term stability for more than 100 h at 400 mA cm^{-2} in the membrane electrode assembly (MEA) electrolyzer. Moreover, recent findings indicate the formation of abundant Pb-rich Cu GB sites on the reconstructed Pb-doped Cu catalyst, effectively increasing *CO surface coverage on the Cu surface.[97] The structurally flexible Pb-Cu catalyst possessed a high conversion of CO to n-propanol with an FE of 47% and a half-cell energy conversion efficiency (EE) of 25% in a flow cell. Besides, a stable FE above 30% of n-propanol production with a full-cell EE of over 16% was maintained for over 100 h in the MEA electrolyzer. In the dynamic reoxidation-reduction process, the atomic interdiffusion of Cu and Ag on a bimetallic $Cu_{68}Ag_{32}$ nanowire promoted the formation of CuAg alloy. The reconstructed CuAg alloy phase not only mitigated the reoxidation of Cu but also induced tensile strain with optimized d-band center, which enhanced the bonding of *CHO intermediates for CH_4 production.[98] A similar reconstruction process was observed on an epitaxial Au-Cu heterostructure, which was dynamically restructured from phase-separated bimetals to AuCu alloy-supported core-shell nanoclusters through the oxidation-reduction of Cu at the interface.[99] Recent studies revealed that Cu atoms in AgCu catalyst exhibited high mobility under CO_2RR conditions.[100–102] Cu atoms could migrate to the catalyst surface, detach from the catalyst, and aggregate into new particles. The separation of Cu and Ag contributed to the formation of AgCu phase boundaries with Cu-rich and Ag-rich grains. The metallic Cu state in the AgCu catalyst acted as the catalytic active sites for CO_2RR.[102]

Other efforts to trigger the surface reconstruction of pre-catalysts have been made by incorporating non-metallic elements, such as halogen, sulfur, nitrogen, phosphor, and boron.[25,103] In contrast to the active components introduced by metal doping, the incorporation of non-metal atoms usually creates defect sites and alters the surface roughness of the reconstructed catalysts.[104,105] Copper halide catalysts containing halogens (e.g., F, Cl, Br, and I) have been extensively investigated for electrocatalytic CO_2RR toward C_{2+} production.[24,106] For instance, Wang's group presented a fluorine-modified copper catalyst prepared by the electroreduction of a Cu(OH)F precursor, achieving highly active and selective C_{2+} generation through hydrogen-assisted C-C coupling reaction. The presence of F anion on the Cu surface promotes H_2O activation through interaction with hydrated cations. The F modification also increases surface $Cu^{\delta+}$ sites, enhancing the CO adsorption and the subsequent hydrogenation to CHO intermediates.[107] Similarly, the Cu_KX (X = Cl, Br, and I) catalysts, obtained by anodic halogenation, oxidation, and electroreduction process (Figure 7A), undergo abrupt changes in morphology and chemical composition. This

process generates a high density of under-coordinated atoms on the surface of the reconstructed Cu_KX catalysts, fostering CO_2RR toward C_{2+} products by suppressing HER and C_1 production.[74] Furthermore, iodide-derived Cu (ID-Cu) catalyst is capable of altering localized geometry by adjusting defect density (residual I ions, Cu^+, and uncoordinated Cu) and surface roughness, influencing the CO_2RR pathways. The high-density defects of residual I ions or Cu^+ alter the d band center of Cu sites, thereby strengthening the adsorption of *CO intermediates. Moreover, increased surface roughness prolongs the residence time of *C-H intermediates and reduces the formation energy of *OCOC and $*CH_3CH_2O$ intermediates, thus facilitating the production of C_{2+} compounds.[108] Another example is CuI per-catalyst prepared by anodizing Cu island in a KI-containing solution. CuI was reduced back to Cu under CO_2RR conditions. The morphology of Cu transferred from islands to fragmented filaments during the dynamic reconstruction process, favorable for the stabilization of Cu^+ species. The stable Cu^+ species in the filamentous structure led to the formation of Cu^+/Cu interfaces, which improved the selectivity of C_{2+} products.[109] Aside from halogen atoms, Cu catalysts derived from electrochemically reconstructed heteroatom-incorporated pre-catalysts have also shown promise in promoting C-C coupling for C_{2+} production. For example, Qiao's group reported that Cu-based compounds with nonmetallic atoms (Cu_nX, X = N, P, S, and O) can be reduced to heteroatom-engineered Cu (X-Cu) catalysts with significant structural reconstruction under CO_2RR. The type of heteroatoms had a profound influence on the selectivity of CO_2RR, in which the N-Cu catalyst achieved ampere-level current densities of CO_2RR to C_{2+} products with an FE of over 70% at −1.15 V in a flow cell (Figure 7B). Notably, *CO adsorption was greatly enhanced on N-tailored Cu sites in the N-Cu catalyst (Figure 7C), ensuring sufficient *CO coverage to accelerate the C-C coupling rate.[110]

The incorporation of high-electronegative non-metal atoms into metals can effectively modulate the adsorption ability of the key intermediates, particularly in the production of formate, through electronic structure modulation. One such example is the generation of active S-adsorbed Cu sites via the electrochemical reduction of S-doped Cu_2O catalysts during the CO_2RR. This process leads to the creation of S-adsorbed Cu surfaces, which stabilize the crucial *OCHO species while inhibiting the adsorption of *H and *COOH intermediates. Consequently, this facilitates the CO_2RR toward formate production.[111] In addition to Cu-based materials, main-group metals also exhibit high activity and selectivity in CO_2 conversion to formic acid/formate. Mai's group reported the electrochemical reconstruction of $Bi_{19}Br_3S_{27}$ pre-catalyst into Bi nanosheets, where edge defect sites coordinated with S promote CO_2RR selectivity toward formate production. The binding of S to the Bi edge site functions to reduce coordination-unsaturated Bi sites for *H adsorption and regulate the electronic states of neighboring Bi sites for enhancing *OCHO adsorption.[104] Similarly, the valence state of Sn catalysts can be effectively increased after halogen incorporation, which augments the adsorption of key *OCHO intermediate for selective CO_2RR toward formate, while concurrently suppressing the adsorption of *H and *COOH intermediates.[112] These modifications in catalyst composition show promise in influencing the selectivity and efficiency of CO_2RR toward formate generation.

Electrolyte effect

The electrocatalytic reaction occurs at the electrode-electrolyte interface, where electrolyte properties play a pivotal role in CO_2RR performance. The local electrolyte microenvironment at the catalyst surface undergoes dynamic changes during CO_2RR, prompting dynamic reconstruction of the catalyst. These electrolyte-induced changes can lead to variations in morphology and composition, creating active catalytic sites on the surface. These sites are just as important as those caused by the potential-driven reconstructing of intrinsic catalyst structures. Recent studies have explored the significance of electrolyte-derived surface reconstruction during CO_2RR, revealing the substantial impact of electrolyte cations and anions on the activity and selectivity of the CO_2RR process.[113,114] For instance, the coexistence of Cs^+ cation and I^- anion in the electrolyte promotes dynamic reconstructing of the CuO_x surface, fostering more stable Cu^+ species during the reaction and enhancing C_{2+} selectivity.[115] Similarly, surface reconstruction of Ag foils in choline halide solutions leads to morphological evolution and increased surface roughness, culminating in high CO_2 to CO selectivity.[116]

The pH of the electrolyte has greatly influenced the surface reconstruction of the catalyst, steering the CO_2RR reaction pathway and selectivity of products. With the reaction between CO_2 and OH^-, the concentrations of HCO_3^- and CO_3^{2-} in the electrolyte undergo fluctuation, resulting in changes in local pH near the electrode surface.[117,118] Importantly, the change of local pH has a great effect on the dynamic reconstruction of the catalyst.[119,120] For instance, pH-induced surface reconstruction of polycrystalline Cu electrode leads to the formation of oxygen-containing surface phases such as $CuO_x/(OH)_y$ and $Cu_2CO_3(OH)_2$, which changes the preferential binding site of adsorbed CO on the Cu electrode.[120] Conversely, the morphology evolution of the catalyst altered by the dynamic surface reconstruction causes variation in local pH. Jiang et al. found that the Cu_2O superparticles underwent complicated structural evolution under CO_2RR conditions.[121] The building blocks inside the superparticles fused to generate numerous GBs, while those in the outside shell detached to form many nanoscale or sub-nanoscale spacings between Cu facets. This nanogap structure could efficiently confine OH^- to produce high local pH, leading to achieving superior performance for C_{2+} production with a high FE of 74.2%. The reconstruction-induced phase transition also changes the local pH of the reaction microenvironment in the electrolyte. A good example is the dynamic evolution of a Bi-based catalyst under acidic CO_2RR conditions.[122] In a long-term stability test of acidic CO_2RR, the pristine BiOCl catalyst was degraded by reduction and dechlorination reactions, reacted with CO_2 and OH^- to form the $Bi_2O_2CO_3$ transient phase, and then completely reduced to the Bi phase. Because the competitive adsorption between the K^+ and proton was affected by the surface charge property of the dynamic catalyst, the local pH changed from neutral to acid during the dynamic evolution of BiOCl to Bi, resulting in the FE of HCOOH dropping from 91 to 34% within 10 h. To improve the stability of acidic CO_2RR, a pulsed electrolysis technique was developed to regenerate the original phase of the BiOCl catalyst in a chloride-containing electrolyte. This finding suggests that pulsed electrolysis can regulate the dynamic reconstruction of active catalysts by preventing poisoning or degradation. Although the trend of local pH is not given, local pH also can be modulated by pulsed potentials. More on pulsed electrolysis will be discussed in the subsequent Section 3.3.

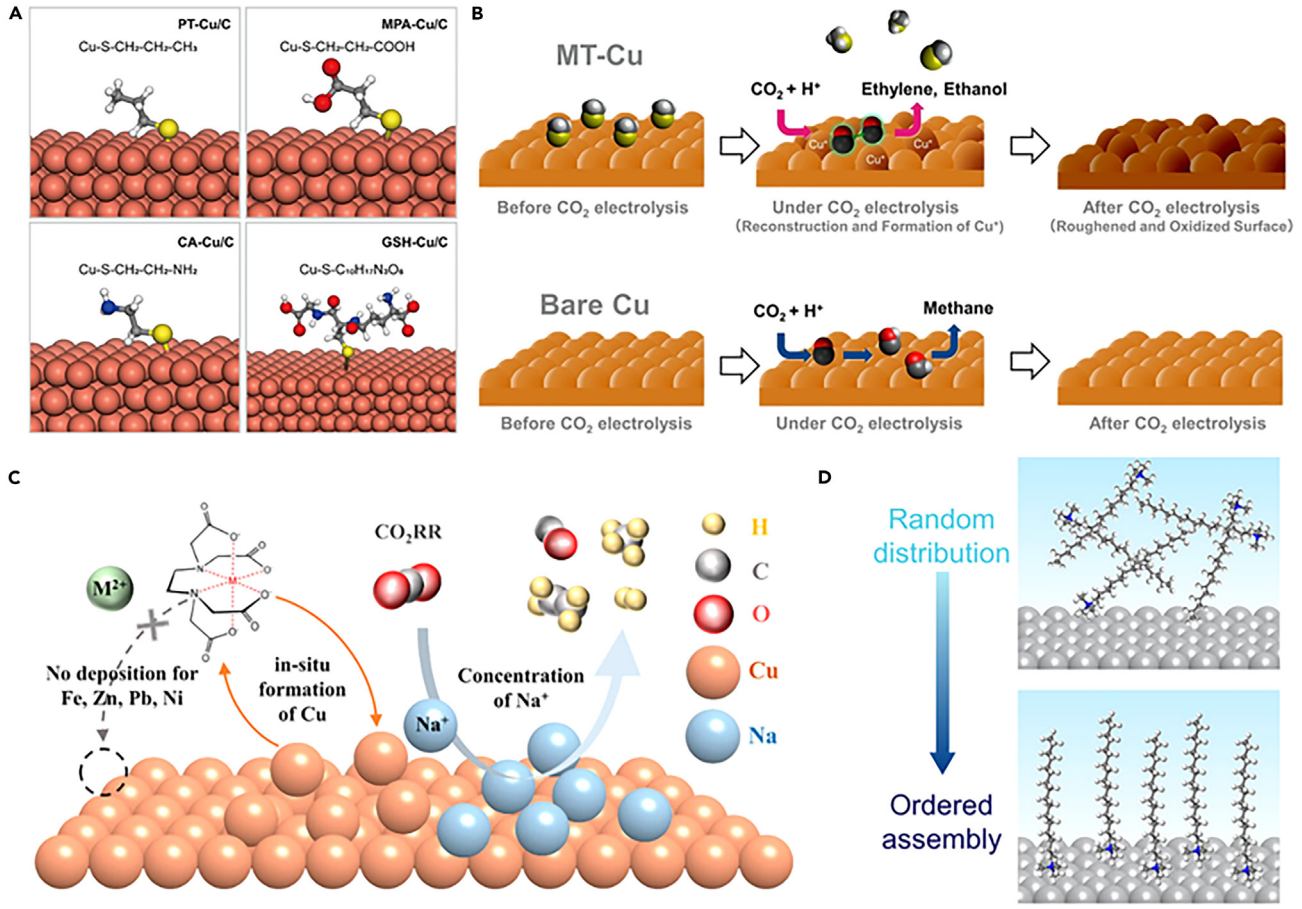

Figure 8. Electrolyte-induced reconstruction

(A) Structures of PT-, MPA-, CA-, and GSH-functionalized Cu Catalysts. Reproduced with permission.[128] Copyright 2022, American Chemical Society.

(B) Schematic illustrations of possible reactions on the MT-Cu and pure Cu electrodes. Reproduced with permission.[129] Copyright 2020, American Chemical Society.

(C) Schematic of *in situ* formation of a Cu catalyst. Reproduced with permission.[131] Copyright 2023, American Chemical Society.

(D) Schematic illustration of surfactant configuration at the electrified interface. Reproduced with permission.[132] Copyright 2022, American Chemical Society.

Molecular modification strategies offer an effective route to functionalize the surface atoms of metal catalysts.[123,124] Particularly, adding organic ligands to electrolytes is a common method for surface functionalization of metal catalysts.[125–127] Shi et al. utilized glutathione ligands to modify Cu catalyst, influencing the local microenvironment at the Cu surface through ligand functional groups (Figure 8A). The carboxyl and amino groups regulate the *CO adsorption configurations and local *H concentration, thus promoting the protonation of *CO to CH_4.[128] Similarly, modifying Cu electrodes with methanethiol monolayers induced reconstruction, forming Cu^+ species on the roughened Cu surface (Figure 8B), which enhances *CO adsorption and dimerization to C_{2+} products.[129] Surfactants have also been used as electrolyte additives to regulate the interfacial microenvironment at the electrode-electrolyte interface.[130] For example, adding ethylenediamine tetraacetic acid disodium salt (EDTA) to the sea salt electrolyte resulted in dendritic Cu catalyst formation with a rougher surface and active sites favoring highly selective CO_2RR toward C_2H_4 production (Figure 8C).[131] Apart from the regulation of the catalyst reconstruction, the surfactant itself can be constructed into a specific structure during the CO_2RR process. Ge et al. demonstrated that quaternary ammonium cationic surfactant underwent dynamic structural evolution, transitioning from a random distribution to a nearly ordered assembly at the electrified electrode-electrolyte interface (Figure 8D). Such an ordered surfactant assembly establishes an aerophilic-hydrophobic interfacial microenvironment on the Ag electrode surface, contributing to decreasing water dissociation activity and thus boosting CO_2RR selectivity toward CO.[132]

Pulsed electrolysis

Pulsed electrolysis techniques have been developed as a novel approach for CO_2RR toward a target product with enhanced selectivity and stability.[133] The benefits of pulsed electrolysis over conventional steady-state (potentiostatic/galvanostatic) electrolysis are mainly reflected in the control of the oxidate state of the catalysts and the local pH environment near the catalyst surface.[134] Generally, the application of a periodic oxidative potential to the electrolysis process can induce the reoxidation of the catalyst after the reductive pulse, thus triggering the

dynamic reconstruction of the catalyst. Especially for oxidates, pulse electrolysis is also beneficial to the regeneration of the catalyst and improves the catalytic stability.[135] Consequently, the surface dynamics can be modified by local reaction environment through pulsed electrolysis that regulate of concentration of H^+, OH^- ions and the coverage CO or carbonate, resulting in the changeable of CO_2RR selectivity.[136–138]

Starting in the 1990s, pulsed electroreduction of CO_2 was performed on Cu electrodes, and the FEs of CH_4 and C_2H_4 gaseous products were constant during the long-term electrolysis process.[139] But for galvanostatic electroreduction, the Cu electrode may be poisoned, resulting in an inevitable sharp decline in FEs. Following the Cu electrode, other electrodes such as Ag and Cu-Ag alloy were employed for pulsed CO_2 electroreduction, also showing improved selectivity compared to galvanostatic electroreduction.[140,141] However, the exact reason for the difference in selectivity between pulsed and galvanostatic electroreduction was not clear at that time. The researcher later found that the formation of an oxide layer on the metal surface through anodic polarization during pulsed electrolysis helped prevent poisoning or deactivation of the metal electrode.[142,143] With further study of the pulsed electrolysis, the enhanced selectivity of CO_2RR could be attributed to the suppression of hydrogen evolution reaction by controlling pulsed duration. The pulsed potential leads to a rearranged surface coverage of hydrogen and CO_2-related intermediates (CO and carbonate) on the catalyst surface.[144–146] The dynamic changes of local pH and CO_2 concentration near the electrode under pulsed potential also affect the product selectivity of CO_2RR.[147] These emerging studies suggest that pulsed electrolysis can change the reaction environment near the catalyst surface and regulate the adsorption ability of the reaction intermediates, thereby improving the selectivity and durability of CO_2RR.

The pulse can adjust the active components of the catalysts through dynamic reconstruction. Since pulsed electrolysis usually involves oxidation (at anodic potential) and reduction (at cathodic potential) reactions, the catalysts will undergo structure reconstructing during the redox process. The concomitant presence of morphological features, electrochemically active surface area, exposed facets, and composition factors should be also considered at the same time. The significant advantage of pulsed electrolysis is that the anodic potential and duration can be reasonably adjusted to obtain oxidation state species on the catalyst surface.[105,148] The *in situ* formed partially oxidized species could switch the adsorption ability from *H to carbonaceous intermediates, which facilitates the achievement of highly selective CO_2RR performance. Particularly, for the Cu catalysts, the stabilized Cu^+ species by the pulsed electrolysis combined with Cu^0 site synergetic promote CO_2 reduction to C_{2+} products.[149] Cuenya et al. observed the evolution of the morphology and composition on a Cu (100) electrode under pulsed electrolysis conditions. The *ex situ* AFM showed that the continuous oxidation and reduction of Cu resulted in cubic islands creating some step-edge defects. The dynamic applied anodic and cathodic potential led to the partial oxidation of the Cu (100) surface to create stable Cu^+ species, as revealed by quasi-*in situ* XPS. The defects and the stable Cu^+ species derived from structure evolution on the Cu (100) surface synergistically promote the reduction of CO_2 to C_{2+} products.[150] They further studied the dynamic balance between the oxidized and reduced surface species on Cu_2O nanocubes by adjusting the pulsed durations. The average concentration of Cu(I) and Cu(II) species and their ratios were closely related to anodic pulse duration (Δt_a) and cathodic pulse duration (Δt_c). At a larger Δt_c, the Cu_2O was completely reduced to metallic Cu, and the FEs of the products was similar to those under static CO_2 reduction. As the Δt_c decreased, the oxide species were created on the catalyst surface and their fractions were affected by the Δt_a, which steered the product distribution of CO_2RR.[17] Li et al. found that pulsed electrolysis can regulate the selectivity of CO_2RR by controlling the surface Cu_xO/Cu composition and reaction intermediates (Figure 9A). *In situ* Raman spectra have well demonstrated that Cu_2O species were formed during the anodic duration and rapidly reduced to metallic Cu at the cathodic potential. However, the adsorption of CO on the catalyst surface could be only detected during the cathodic duration. Consequently, a volcano shape dependence between the CO adsorption and the surface Cu_xO/Cu ratio was achieved by controlling the duration of anodic/cathodic potential. The optimal surface Cu_xO/Cu ratio was favorable for CO adsorption, thus adjusting the selectivity of CO_2RR.[151] Besides, the Cu complex catalysts also undergo structural reconstruction under electrochemical CO_2 reduction conditions. Usually, the Cu complex would be constructed into the Cu clusters during the reaction. Zhang et al. found that the oxidation state of Cu in the Cu-dimethylpyrazole complex-based clusters could be modulated by tailoring the asymmetric duration of anodic/cathodic potential in pulsed electrolysis (Figure 9B). The oxidation state of Cu^+ in the Cu clusters favored the C_2H_4 product and the mixed Cu^+ and Cu^{2+} species were conducive to CH_4 production. It is also worth noting that the periodic oxidation process in the pulsed electrolysis could prevent the aggregation of Cu-based clusters, thereby improving the stability of CO_2RR.[152]

In situ/operando techniques for analyzing reconstruction

The dynamic reconstruction of catalysts presents a formidable challenge in comprehending the structural evolution, chemical states, and reaction intermediates involved in CO_2RR. *In situ*/operando characterization techniques serve as invaluable tools offering tangible evidence for surface evolution of catalysts under operational conditions. Advancement *in situ*/operando spectroscopy particularly provides a robust means to monitor intermediates and reaction steps in CO_2RR. This section aims to provide a summary of utilizing *in situ*/operando techniques to uncover the dynamic reconstruction process of catalysts under CO_2RR conditions.

Monitoring morphological evolution

Morphological change is a hallmark of reconstructed behavior that has garnered significant attention from researchers. Cutting-edge *in situ*/operando electrochemical microscopy techniques, such as SEM, AFM, TEM, and STM, are utilized to monitor the evolution of morphological structure under potential-driven CO_2RR conditions. For example, *in situ* electrochemical SEM images reveal the transformation of an electrodeposited Cu electrode from a smooth surface to a rough one, characterized by crevices and channels, thus creating numerous uncoordinated sites that augment CO_2RR activity and selectivity.[153] Employing *in situ* electrochemical AFM techniques, Cuenya's group observed the morphological transformation of the Cu surface during CO_2RR.[150,154–156] As the potential shifts from −0.5 V to −1.0 V, the surface

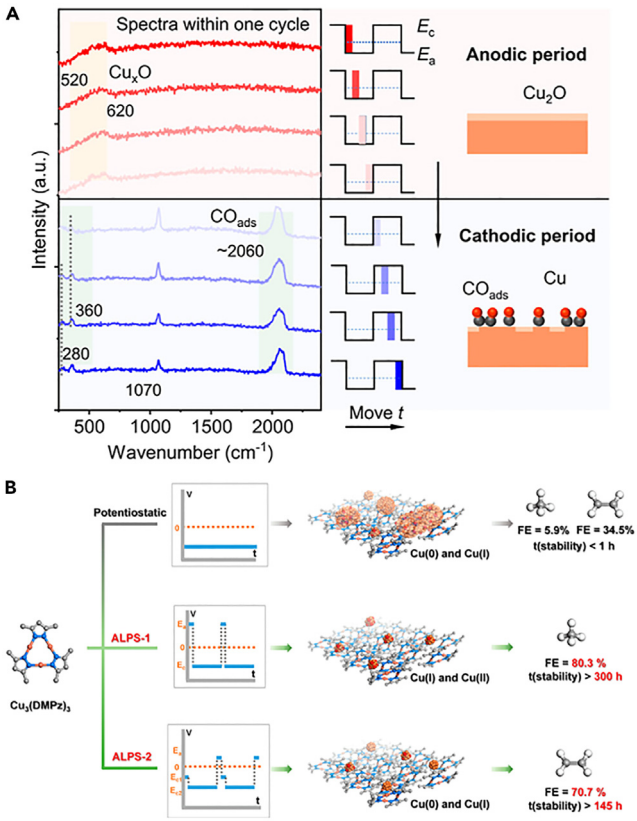

Figure 9. Pulsed electrolysis for dynamic reconstruction

(A) *In situ* Raman spectra of Cu during pulsed electrolysis of CO reduction. Reproduced with permission.[151] Copyright 2023, American Chemical Society.

(B) Scheme illustration of asymmetric low-frequency pulsed strategy for the Cu complex catalysts. Reproduced with permission.[152] Copyright 2023, American Chemical Society.

morphology transitions from a mound-pit structure with atomic-scale terraces and steps to straight terrace edges with right angles (Figure 10A).[155] *In situ* TEM analysis allows real-time monitoring of morphological changes in Cu nanoparticles, including immediate shape, size, and crystal structure. A proposed dissolution and redeposition mechanism during the initial state of CO_2RR involves the generation of Cu ions from the dissolution of Cu_2O under open circuit conditions. These Cu ions are then released into the electrolyte, reduced to Cu, and redeposited onto the working electrode, leading to an apparent growth in particle size under constant reduction potential.[157] Similarly, potential-driven morphological changes in Cu single-atom catalysts result in the reconstruction into Cu clusters (Figure 10B), generating dynamic low-coordinated configuration sites that efficiently catalyze CO_2-to-CO conversion.[158] Operando electrochemical STM techniques have also been developed to scrutinize the atomic-scale surface restructuring of Cu-based CO_2RR catalysts.[61,159] By employing *in situ* STM, the nanoclustering phenomenon on the Cu (100) electrode under CO_2RR conditions was observed, as shown in Figure 10C. These nanoclusters formed near the onset potential of CO_2 reduction and disappeared as the potential returned to the positive range. Through combined *in situ* STM and Raman spectroscopy results, a mechanism was proposed where the ordered carbonate adlayer on a smooth Cu surface becomes disordered at a potential below 0 V, forming carboxylate intermediates. A further potential decrease to below −0.2 V reduces these intermediates to CO, inducing the formation of Cu adatoms and surface vacancies, ultimately leading to the development of Cu nanoclusters and vacancy islands. These nanoclusters persist on the surface at larger negative potentials but decay to isolated adatoms when the potential returns above −0.2 V. This dynamic restructuring process results in the irreversible formation of low-coordinated Cu surface species, closely associated with specific CO_2RR reaction pathways.[160]

Identifying composition and surface states

The dynamic surface reconstruction of catalysts often induces changes in composition and surface chemical states, which are also directly associated with the activity and selectivity of CO_2RR. Under CO_2RR conditions, phase transitions and surface oxidation in reconstructed catalysts have been widely observed through *in situ* XRD, XPS, XAS, and other techniques.

Several operando spectroscopy studies have delved into the structural evolution of Cu-based materials, examining the transformation of crystal phases, chemical components, and surface-active species. For instance, on single-crystal Cu foil, operando grazing incidence XRD revealed surface evolution-induced crystal facet formation (Figures 11A and 11B). The Cu(111) and Cu(110) crystal facets maintained stable

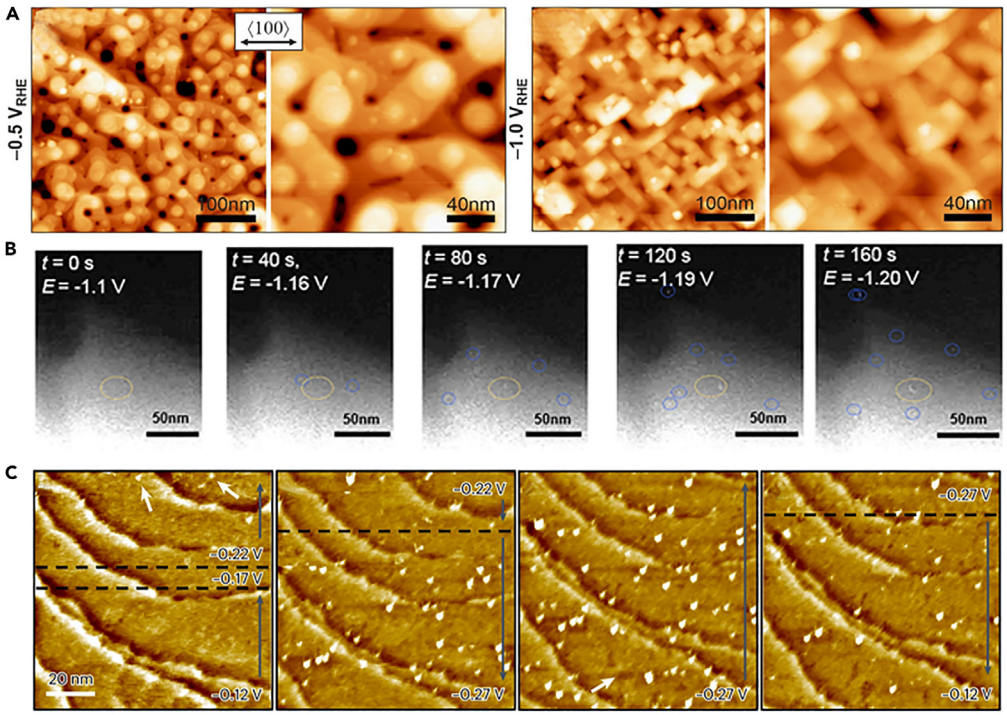

Figure 10. *In situ* characterization of morphology evolution

(A) *In situ* AFM images of a Cu(100) electrode after different surface treatments and reaction settings. Reproduced with permission.[155] Copyright 2020, Wiley-VCH.

(B) Dark-field STEM images at truly calibrated potentials vs. RHE with various durations from 0 to 160 s. Reproduced with permission.[158] Copyright 2023, Springer Nature.

(C) Sequence of *in situ* STM images recorded during stepwise potential changes. Reproduced with permission.[160] Copyright 2023, Springer Nature.

during electrocatalytic CO_2RR at a potential of −1.15 V for 3 h, while the Cu(100) facet experienced a partial structural transformation from Cu(100) to Cu(111) and the ratio of Cu(111) stabilized at 15% after 3-h electrolysis. Supplementary electron back-scattered diffraction (EBSD) analyses facilitated estimations of intrinsic structure-function correlations, employing descriptors such as crystal facets, atomic coordination numbers, and step-terrace angles.[161] Electrochemical reduction-oxidation-reduction pretreatment induces the reconstruction of Cu catalysts, resulting in the formation of abundant undercoordinated Cu sites, oxygen vacancies, and grain boundary-derived Cu/Cu_2O interfaces. Particularly, *in situ* synchrotron powder diffraction and Raman measurements showcased the dynamic transition of Cu species from CuO phase to Cu_2O and metallic Cu.[62] Operando XAS and quasi-*in situ* XPS measurements revealed a reversible transformation from dispersed CuO clusters to Cu_2-CuN_3 moieties (Figures 11C–11G). These *in situ*-generated Cu_2-CuN_3 clusters act as highly dispersed charge-asymmetric sites, promoting the formation of asymmetric ethanol with FE up to 51% and a partial current density of 14.4 mA cm^{-2} at −1.1 V in CO_2-saturated 0.1 M $KHCO_3$ solution.[162] Moreover, Cu-based catalysts also undergo dynamic reconstruction of the oxidation states during CO_2RR. *In situ* grazing incidence XAS and XRD results provided evidence of the complete reduction of the near-surface region of polycrystalline Cu thin films, transitioning to metallic Cu with the surface reconstruction of Cu (100) in the presence of CO_2.[66]

The dynamic structural evolution of other metal-based catalysts was also detected by *in situ*/operando techniques. *In situ* XRD and XAS tests confirmed the transformation of metallic Pd catalyst into β-PdH phase during CO_2RR. This active β-PdH phase exhibited weaker adsorption of *CO and *H, resulting in a highly selective reduction of CO_2 to syngas.[163] Furthermore, halides were found to promote the reconstruction of bismuth oxyhalide (BiOX) into metallic Bi catalyst in the electrochemical CO_2RR process. *In situ* XRD measurements revealed that the selective facet exposure of Bi catalyst was significantly influenced by the type of halide (Figures 12A–12C). The Br promotes the exposure of Bi (003) while Cl and I guide the reconstruction to favor Bi (012) surface. Bi (003) exhibited higher activity and selectivity toward formic acid than Bi (012). This halide-guided facet exposure was correlated with the reconstruction rate of BiOX, as demonstrated by *in situ* XAS spectroscopy (Figures 12D–12F).[164] Observations of phase transition were also made in Ag-based catalysts during the electrochemical reconstruction process. Taking Ag hollow fiber (Ag HF) as an example, the electrooxidation process forms an AgCl nanosheet layer on the outer surface, followed by transforming into an Ag nanosheet shell through *in situ* electroreduction. The *ex situ* XRD and operando Raman results clearly demonstrated these phase transition processes between AgCl and Ag compositions during *in situ* reconstruction of the Ag HF catalyst.[165] The surface morphology and chemical state of the SnO_x/AgO_x catalyst at different reduction conditions were monitored by quasi-*in situ* XPS and operando X-ray absorption near-edge structure spectroscopy (XANES). The stable $Sn^{\delta+}$/Sn species formed on the SnO_x/AgO_x surface acted as a key site for CO_2RR, resulting in high selectivity and long-term CO_2-to-CO and formate conversion with a total FE of 95%.[166]

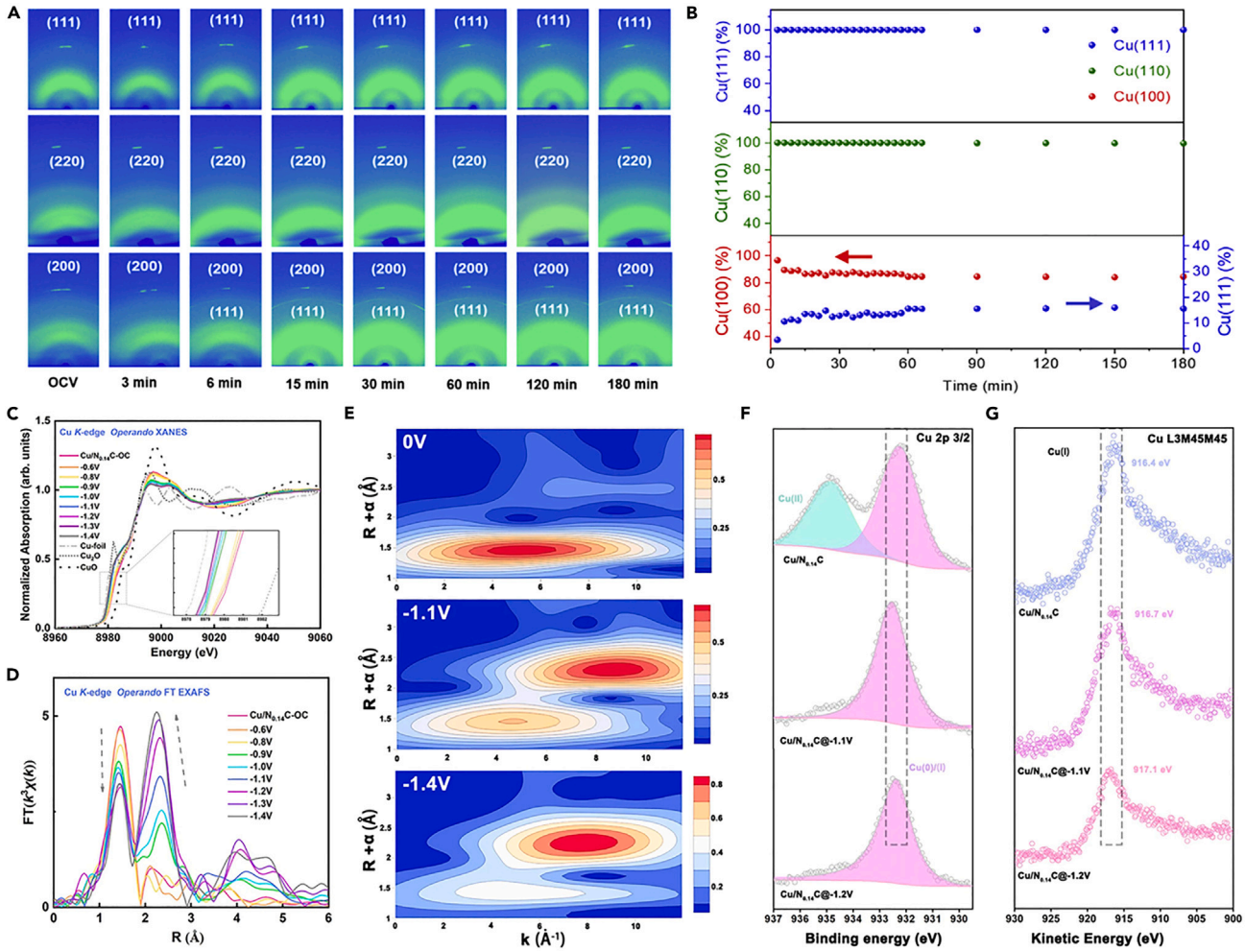

Figure 11. *In situ*/operando analysis of composition and chemical state

(A) Operando GIXRD images and (B) quantitative analysis of Cu(111), Cu(110), and Cu(100) under CO_2RR. Reproduced with permission.[161] Copyright 2021, Cell Press.

(C–E) Operando XAFS characterization of Cu/$N_{0.14}$C. Quasi-*in-situ* XPS of (F) Cu $2p_{3/2}$ and (G) Cu LMM for Cu/$N_{0.14}$C. Reproduced with permission.[162] Copyright 2022, Springer Nature.

Detecting reaction intermediates

The electrochemical reconstruction of catalysts generates multiple active sites, influencing the adsorption patterns of key intermediates, and finely tuning the activity and selectivity of CO_2 reduction. To gain a comprehensive understanding of the CO_2RR mechanism toward a specific product, it is essential to explore and characterize the adsorbed species and reaction intermediates on the reconstructed catalyst surface. In recent years, the development of various advanced *in situ*/operando spectroscopic techniques has provided direct and valuable methods to investigate these reaction intermediates.

Operando Raman spectroscopy has proven invaluable in not just identifying catalyst composition and phase evolution, but also in unraveling critical information about the adsorbed reaction intermediates on the catalyst surface during catalytic reaction.[167–169] Regarding CO_2RR activity, particularly in C_{2+} production on Cu catalyst surfaces, the adsorption of *CO intermediate plays a pivotal role.[170] By detecting the rotation and stretching bands of *CO intermediates adsorbed Cu surface (Cu-CO) at wavenumbers of about 280 and 365 cm^{-1}, Sargent's group found that the onset potential of *CO formation on the molecule-immobilized Cu (e.g., FeTPP[Cl]/Cu) electrode was lower than that of pure Cu electrode. The additional Fe-CO bending vibration signal on the FeTPP[Cl]/Cu electrode was related to the interaction between CO and Fe in the iron porphyrin segment, which proved that a high concentration of *CO was produced on the molecule-metal catalyst interfaces, thus providing sufficient CO supply for the C-C coupling to ethanol.[171] Analyzing *in situ* Raman data across various studies reveals intriguing patterns. For instance, the peak intensity ratio of *CO rotation and stretching bands demonstrates a volcano-type trend concerning applied potential.[172] Higher intensity ratios of *CO stretching to *CO rotation tend to have higher FE of C_{2+} products.[173] Aside from the Cu-CO rotation and stretching bands, the C≡O stretching vibration of *CO intermediates also can be detected in the Raman spectra within the

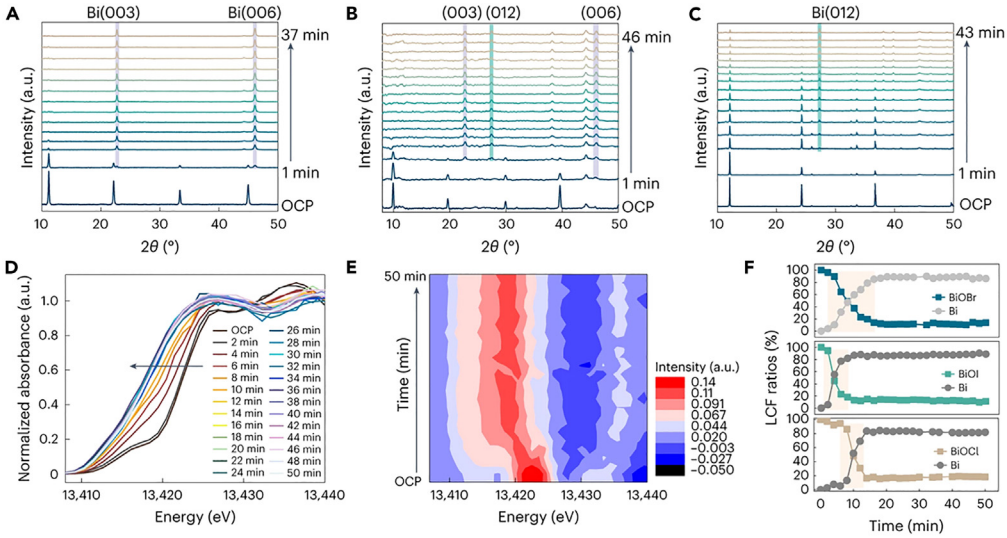

Figure 12. *In situ*/operando characterization of other metal-based catalysts

(A–C) Time-dependent *in situ* XRD patterns of (A) BiOBr, (B) BiOI and (C) BiOCl during CO_2RR.

(D) Time-dependent *in situ* XANES spectra of BiOBr.

(E) The heatmap of corresponding first derivative.

(F) Corresponding linear combination fitting results. Reproduced with permission.[164] Copyright 2023, Springer Nature.

range of 1900–2100 cm^{-1}.[169,174] These C≡O stretching bands typically comprise bridge-bound CO (CO_{brigde}) and atop-bound CO (CO_{atop}), with CO_{atop} further subdivided into terrace site-related low-frequency binding *CO (CO_{LFB}) and defect site-related high-frequency binding *CO (CO_{HFB}) adsorption.[175,176] Sargent's group discovered a volcano-shaped relationship between ethylene selectivity and the ratio of CO_{atop} to CO_{bridge} band intensity.[177] Additionally, they highlighted a linear relationship between C_{2+} selectivity and the ratio of CO_{LFB} to CO_{HFB} band intensity on various alkaline earth metal oxide/Cu catalysts, indicating that CO_{LFB} significantly contributes to C_{2+} production.[178] In short, the band intensity of adsorbed *CO intermediate in the Raman spectra showcases CO coverage while the band position reflects the CO adsorption configuration and the adsorption sites, both exerting influence over the product's selectivity, particularly in C-C coupling reactions on Cu catalysts.

The local environment surrounding the catalyst surface, including local pH, significantly influences the activity and selectivity of the CO_2RR. In CO_2RR with water as the proton source, OH^- ions are typically generated and then are neutralized by reacting with CO_2 to form bicarbonate (HCO_3^-) and carbonate (CO_3^{2-}). Changes in the equilibrium of these species in neutral or alkaline CO_2 electrolytes can significantly impact the local pH near the electrode/electrolyte interface.[117] Estimating the concentrations of HCO_3^- and CO_3^{2-} can be achieved by integrating peak areas in Raman spectroscopy. The relative peak area ratio of CO_3^{2-}/HCO_3^- provides insights into the surface OH^- concentration.[179] The OH^- near the electrode will be fully consumed by CO_2 to form HCO_3^- and CO_3^{2-}. This chemical reaction between OH^- and CO_2 causes the local pH to be lower than that of the bulk electrolyte. Consequently, the local pH near the gas diffusion electrode surface declines as the distance from the electrode decreases.[180] Using *in situ* Raman spectra, Wu et al. observed that the local OH^- concentration on the tannic acid (TA) molecule-modulated Cu (CuTA) electrode surface surpassed that of CuO nanosheet surface. This heightened OH^- concentration facilitated the adsorption of *CO, thereby enhancing *CO coverage on the reconstructed Cu (100) surface, resulting in elevated CO_2-to-C_{2+} selectivity.[181]

Uncovering the Raman signal of reaction intermediates beyond *CO offers valuable insights into the pathways of the CO_2RR process. In their study utilizing *in situ* Raman spectra (Figure 13A), Liu's group identified two initial intermediates, $*COO^-$ and $*OCO^-$, adsorbed on the nanoporous Ag surface, involving one carbon atom and two oxygen atoms, respectively. The diverse configurations of CO_2 adsorption led to distinct reaction pathways in the subsequent protonation-reduction process (Figure 13B). Pathway I involves *COOH reduction to CO and further C-C coupling to C_2 products, whereas pathway II directs *OCHO transforming into HCOOH. Electrodepositing Cu or Pd on the Ag surface allowed control over reaction pathways, as reflected in the intensity of Raman peaks for $*COOH^-$ and $*OCO^-$. Ag@Cu exhibited a high A_{OCO}/A_{COOH} ratio, favoring pathway I, while Ag@Cu with a low ratio favored pathway II.[182] Later research by the same group indicated that HCO_3^- in the electrolyte promoted the adsorption of $*OCO^-$ over *COOH, thereby regulating the CO_2RR pathway and influencing product distribution.[183] Li's group explored facet-dependent CO_2RR processes by identifying key intermediates, such as *COOH, *CO, *OCCO, and $*CH_2CHO$. Combined findings from *in situ* Raman analyses and theoretical calculations unveiled that the Cu (111) surface favored CH_4 production via the formation of *COOH and *CO, while the Cu (110) surface led to C_{2+} product generation by forming *OCCO and $*CH_2CHO$ intermediates. A high HCO_3^- concentration was conducive to the formation of *OCCO, thereby promoting the generation of C_{2+} products.[184]

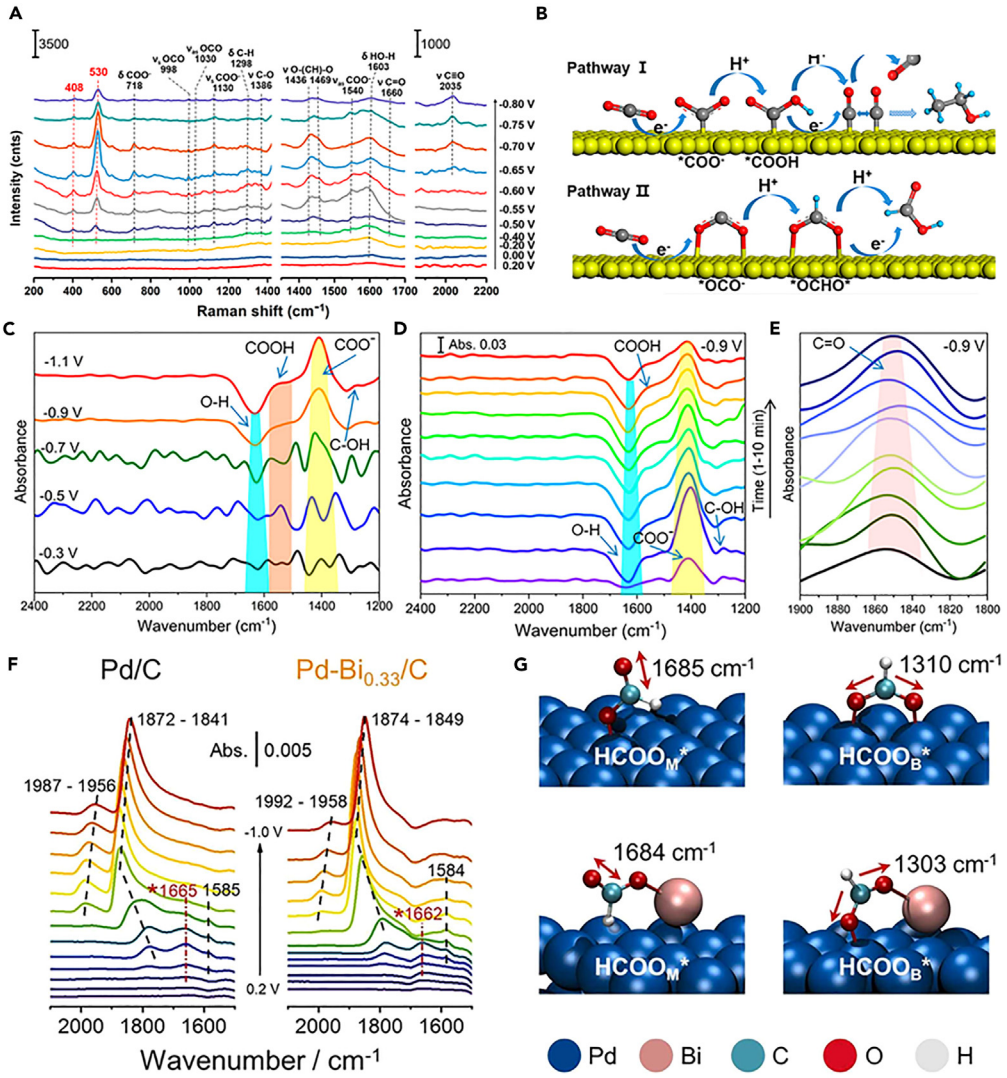

Figure 13. *In situ*/operando spectra for detecting reaction intermediates

(A) *In situ* Raman spectra of CO_2RR at np-Ag surface.

(B) Schematic depiction of two preliminary CO_2RR pathways on np-Ag. Reproduced with permission.[182] Copyright 2020, American Chemical Society.

(C–E) *In situ* infrared spectra of different intermediates adsorbed on a PdIn@In_2O_3 catalyst surface during CO_2RR. Reproduced with permission.[187] Copyright 2020, American Chemical Society.

(F) Potential-dependent ATR-SEIRA spectra for Pd/C and Pd-$Bi_{0.33}$/C.

(G) Configurations and vibrational frequencies for formate adsorbed on Pd(111) and Pd(111)-Bi model surfaces. Reproduced with permission.[192] Copyright 2023, Elsevier.

Operando infrared spectroscopy, complementary to Raman spectroscopy, also tracks the reaction intermediates during CO_2RR.[185] Ag, Au, ZnO, and metal-nitrogen-carbon (M-N-C) single-atom compounds are commonly employed as CO-selective catalysts. During the reduction of CO_2 to CO, the important *COO^-, *COOH, and *CO intermediates are frequently detected on the surface of these catalysts (Figures 13C–13E). The recognized reaction mechanism of CO_2 reduction to CO, as demonstrated by several catalysts such as Ag,[186] PdIn@In_2O_3,[187] Cu/ZnO,[188] and M-N-C,[189] follows the pathway of *CO_2-*COOH-*CO-CO, as measured by operando attenuated total reflection FTIR (ATR-FTIR) studies. The development of HCOO* or OCHO* intermediate, which can be separated from the *COOH intermediate by the FTIR signals, is thought to be the rate-determining step for formate/formic acid production in the CO_2-to-HCOOH pathway.[190] The identification of HCOO* in operando ATR-FTIR spectra provides concrete proof to clarify the formate synthesis reaction process.[191] In contrast to bidentate $HCOO_B$*, Jiang et al. suggested that monodentate bonded HCOO* ($HCOO_M$*) was a dominant intermediate for formate synthesis on the Pd catalyst (Figure 13F). The adsorption of $HCOO_M$* was stabilized by modifying Bi on the Pb surface (Figure 13G), which favored the CO_2-to-HCOOH pathway.[192] Furthermore, *in situ* UV-Vis adsorption spectroscopy can be employed to detect reaction intermediates such as

CO_2^{-}* radical anion in CO_2RR.[193,194] When CO_2RR occurs on Bi nanosheets, the CO_2^{-}* radical concentration increases with increasing applied potential, suggesting that the high adsorption of CO_2 facilitates CO_2 reduction to formate.[195]

Conclusions and perspectives

Electrochemical CO_2RR technology holds promise for converting CO_2 into high-value fuels and chemicals. However, existing catalysts struggle to achieve optimal CO_2RR activity, selectivity, and stability. The dynamic evolution of catalysts further complicates the design of advanced catalysts for CO_2RR. The principles of reconstruction behaviors in electrocatalysis are first discussed in terms of thermodynamics and kinetics. The changes in chemical state or phase of the catalysts and atomic rearrangement with size, shape, and atomic distribution have been reviewed as well as the classification of the catalysts. Then, common strategies for modulating the reconstruction process are discussed, including heteroatom incorporation, electrolyte effect, and pulsed electrolysis. The structural evolution of the catalyst can induce different active sites with distinguished facets, surface oxidation states, interfaces, and defects. The incorporation of heteroatoms can trigger atomic rearrangements and composition changes in the reduction process. The electrolyte may drive reconstruction by interacting with the catalysts to generate new active species while the catalyst reconstruction in turn alters the local environment of the catalyst surface. Pulsed electrolysis with alternative positive and negative potentials can dynamically reconstruct the catalysts to form desired active sites and to effectively avoid the degradation of catalysts. Finally, various advanced electron microscopy and spectroscopy measurements have provided the possibility to trace the structural evolution of catalysts and identify the reaction intermediates adsorbed on the surface sites.

The dynamic evolution of catalysts is not only a common phenomenon in the electrocatalytic CO_2 reduction process, but also in other electrocatalytic synthesis, for example, hydrogen evolution and nitrogen reduction reactions. Investigations into the structural evolution process, the real active site reconstruction, and the reaction mechanisms of reconstructed catalysts for specific reactions are still in their early stages. Despite researchers progressively realizing and extensively investigating the dynamic reconstruction behaviors of catalysts, the application of reconstructed catalysts from the laboratory to industrialization has a long journey ahead. In particular, the dynamic reconstruction of atomic-scale catalysts such as single-atom, dual-atom alloys, and clusters is less clear and more complex than that of other nanoscale catalysts. In this regard, an in-depth understanding of the structural evolution and reconstruction mechanism remains a huge challenge, which requires further development of *in situ* characterization methods to monitor the reconstruction process under operating conditions. Furthermore, the stability of reconstructed catalysts must be considered, as atomic leaching or migration may lead to structural collapse. Hence, for the successful adaptation of reconstructed catalysts to the commercial level, more sophisticated structural and spectroscopic characterization techniques must be developed to accurately establish the relationship between the pre-catalyst's structure and composition and the real active site. These experimental techniques can cooperate with artificial intelligence-driven machine learning to streamline the catalyst design process.

ACKNOWLEDGMENTS

We acknowledge the support from the National Natural Science Foundation of China (52202226, 52172293), Key R&D Projects of Anhui Province (202104b11020016), and China Postdoctoral Science Foundation (2021M701028). We also would like to acknowledge the financial support from the Fundamental Research Funds for the Central Universities (PA2022GDSK0056, PA2022GDSK0050), the University Synergy Innovation Program of Anhui Province (GXXT-2022-016) and the 111 Project (B18018).

AUTHOR CONTRIBUTIONS

Writing-Original Draft: J.F.Z.; Formal Analysis: S.X.; Conceptualization, Writing-Review & Editing: J.J.W.; Funding Acquisition: Y.W.; Supervision: J.J.W. and Y.C.W.

DECLARATION OF INTERESTS

The authors declare no competing interests.

REFERENCES

1. Li, X., Zhao, X., Liu, Y., Hatton, T.A., and Liu, Y. (2022). Redox-tunable Lewis bases for electrochemical carbon dioxide capture. Nat. Energy *7*, 1065–1075. https://doi.org/10.1038/s41560-022-01137-z.
2. Madhu, K., Pauliuk, S., Dhathri, S., and Creutzig, F. (2021). Understanding environmental trade-offs and resource demand of direct air capture technologies through comparative life-cycle assessment. Nat. Energy *6*, 1035–1044. https://doi.org/10.1038/s41560-021-00922-6.
3. Shin, H., Hansen, K.U., and Jiao, F. (2021). Techno-economic assessment of low-temperature carbon dioxide electrolysis. Nat. Sustain. *4*, 911–919. https://doi.org/10.1038/s41893-021-00739-x.
4. Wu, Y., Jiang, Z., Lu, X., Liang, Y., and Wang, H. (2019). Domino electroreduction of CO_2 to methanol on a molecular catalyst. Nature *575*, 639–642. https://doi.org/10.1038/s41586-019-1760-8.
5. Zhong, M., Tran, K., Min, Y., Wang, C., Wang, Z., Dinh, C.T., De Luna, P., Yu, Z., Rasouli, A.S., Brodersen, P., et al. (2020). Accelerated discovery of CO_2 electrocatalysts using active machine learning. Nature *581*, 178–183. https://doi.org/10.1038/s41586-020-2242-8.
6. Liu, J., Zhang, X., Yang, R., Yang, Y., and Wang, X. (2023). Electrocatalytic reduction of CO_2 to value-added chemicals via C–C/N coupling. Adv. Energy Sustain. Res. *4*, 2200192. https://doi.org/10.1002/aesr.202200192.
7. Gu, J., Liu, S., Ni, W., Ren, W., Haussener, S., and Hu, X. (2022). Modulating electric field distribution by alkali cations for CO_2 electroreduction in strongly acidic medium. Nat. Catal. *5*, 268–276. https://doi.org/10.1038/s41929-022-00761-y.
8. Ji, Y., Chen, Z., Wei, R., Yang, C., Wang, Y., Xu, J., Zhang, H., Guan, A., Chen, J., Sham, T.-K., et al. (2022). Selective CO-to-acetate electroreduction via intermediate adsorption tuning on ordered Cu–Pd sites.

Nat. Catal. *5*, 251–258. https://doi.org/10.1038/s41929-022-00757-8.

9. Kim, J.Y.'., Zhu, P., Chen, F.-Y., Wu, Z.-Y., Cullen, D.A., and Wang, H. (2022). Recovering carbon losses in CO_2 electrolysis using a solid electrolyte reactor. Nat. Catal. *5*, 288–299. https://doi.org/10.1038/s41929-022-00763-w.
10. Kong, S., Lv, X., Wang, X., Liu, Z., Li, Z., Jia, B., Sun, D., Yang, C., Liu, L., Guan, A., et al. (2022). Delocalization state-induced selective bond breaking for efficient methanol electrosynthesis from CO_2. Nat. Catal. *6*, 6–15. https://doi.org/10.1038/s41929-022-00887-z.
11. Esmaeilirad, M., Jiang, Z., Harzandi, A.M., Kondori, A., Tamadoni Saray, M., Segre, C.U., Shahbazian-Yassar, R., Rappe, A.M., and Asadi, M. (2023). Imidazolium-functionalized Mo_3P nanoparticles with an ionomer coating for electrocatalytic reduction of CO_2 to propane. Nat. Energy *8*, 891–900. https://doi.org/10.1038/s41560-023-01314-8.
12. Zhao, Y., Lv, X., Chen, C., Li, K., Wang, Y., Liu, J., Alkayyali, T., Zhang, S., Ning, J., Liang, Y., et al. (2023). Conversion of CO_2 to multicarbon products in strong acid by controlling the catalyst microenvironment. Nat. Synth. *22*, 403–412. https://doi.org/10.1038/s44160-022-00234-x.
13. Bai, H., Cheng, T., Li, S., Zhou, Z., Yang, H., Li, J., Xie, M., Ye, J., Ji, Y., Li, Y., et al. (2021). Controllable CO adsorption determines ethylene and methane productions from CO_2 electroreduction. Sci. Bull. *66*, 62–68. https://doi.org/10.1016/j.scib.2020.06.023.
14. Yang, Y., Louisia, S., Yu, S., Jin, J., Roh, I., Chen, C., Fonseca Guzman, M.V., Feijóo, J., Chen, P.C., Wang, H., et al. (2023). Operando studies reveal active Cu nanograins for CO_2 electroreduction. Nature *614*, 262–269. https://doi.org/10.1038/s41586-022-05540-0.
15. Gao, F., Zhang, Y., You, H., Li, Z., Zou, B., and Du, Y. (2021). Solvent-mediated shell dimension reconstruction of core@shell PdAu@Pd nanocrystals for robust C_1 and C_2 alcohol electrocatalysis. Small *17*, e2101428. https://doi.org/10.1002/smll.202101428.
16. Huang, W., Wang, Y., Liu, J., Wang, Y., Liu, D., Dong, J., Jia, N., Yang, L., Liu, C., Liu, Z., et al. (2022). Efficient and selective CO_2 reduction to formate on Pd-doped $Pb_3(CO_3)_2(OH)_2$: dynamic catalyst reconstruction and accelerated CO_2 protonation. Small *18*, e2107885. https://doi.org/10.1002/smll.202107885.
17. Timoshenko, J., Bergmann, A., Rettenmaier, C., Herzog, A., Arán-Ais, R.M., Jeon, H.S., Haase, F.T., Hejral, U., Grosse, P., Kühl, S., et al. (2022). Steering the structure and selectivity of CO_2 electroreduction catalysts by potential pulses. Nat. Catal. *5*, 259–267. https://doi.org/10.1038/s41929-022-00760-z.
18. Wang, J., Kim, S.-J., Liu, J., Gao, Y., Choi, S., Han, J., Shin, H., Jo, S., Kim, J., Ciucci, F., et al. (2021). Redirecting dynamic surface restructuring of a layered transition metal oxide catalyst for superior water oxidation. Nat. Catal. *4*, 212–222. https://doi.org/10.1038/s41929-021-00578-1.
19. Kibria, M.G., Dinh, C.T., Seifitokaldani, A., De Luna, P., Burdyny, T., Quintero-Bermudez, R., Ross, M.B., Bushuyev, O.S., García de Arquer, F.P., Yang, P., et al. (2018). A surface reconstruction route to high productivity and selectivity in CO_2 electroreduction toward C_{2+} hydrocarbons. Adv. Mater. *30*, e1804867. https://doi.org/10.1002/adma.201804867.
20. Popović, S., Smiljanic, M., Jovanovic, P., Vavra, J., Buonsanti, R., and Hodnik, N. (2020). Stability and degradation mechanisms of copper-based catalysts for electrochemical CO_2 reduction. Angew. Chem. Int. Ed. *59*, 14736–14746. https://doi.org/10.1002/anie.202000617.
21. Frankel, G., Agarwal, A., and Sridhar, N. (2014). Degradation and deactivation of Sn catalyst used for CO_2 reduction as function of overpotential. Electrochim. Acta *133*, 188–196. https://doi.org/10.1016/j.electacta.2014.04.057.
22. Bienen, F., Löwe, A., Hildebrand, J., Hertle, S., Schonvogel, D., Kopljar, D., Wagner, N., Klemm, E., and Friedrich, K.A. (2021). Degradation study on tin- and bismuth-based gas-diffusion electrodes during electrochemical CO_2 reduction in highly alkaline media. J. Energy Chem. *62*, 367–376. https://doi.org/10.1016/j.jechem.2021.03.050.
23. Shen, H., Zhao, Y., Zhang, L., He, Y., Yang, S., Wang, T., Cao, Y., Guo, Y., Zhang, Q., and Zhang, H. (2022). In-situ constructuring of copper-doped bismuth catalyst for highly efficient CO_2 electrolysis to formate in ampere-level. Adv. Energy Mater. *13*, 2202818. https://doi.org/10.1002/aenm.202202818.
24. Li, H., Liu, T., Wei, P., Lin, L., Gao, D., Wang, G., and Bao, X. (2021). High-rate CO_2 electroreduction to C_{2+} products over a copper-copper iodide catalyst. Angew. Chem. Int. Ed. *60*, 14329–14333. https://doi.org/10.1002/anie.202102657.
25. Xue, W., Liu, H., Chen, X., Yang, X., Yang, R., Liu, Y., Li, M., Yang, X., Xia, B.Y., and You, B. (2023). Operando reconstruction towards stable CuI nanodots with favorable facets for selective CO_2 electroreduction to C_2H_4. Sci. China Chem. *66*, 1834–1843. https://doi.org/10.1007/s11426-023-1591-6.
26. Gunathunge, C.M., Li, J., Li, X., Hong, J.J., and Waegele, M.M. (2020). Revealing the predominant surface facets of rough Cu electrodes under electrochemical conditions. ACS Catal. *10*, 6908–6923. https://doi.org/10.1021/acscatal.9b05532.
27. An, H., Wu, L., Mandemaker, L.D.B., Yang, S., de Ruiter, J., Wijten, J.H.J., Janssens, J.C.L., Hartman, T., van der Stam, W., and Weckhuysen, B.M. (2021). Sub-second time-resolved surface-enhanced Raman spectroscopy reveals dynamic CO intermediates during electrochemical CO_2 reduction on copper. Angew. Chem. Int. Ed. *60*, 16576–16584. https://doi.org/10.1002/anie.202104114.
28. Du, R., Wu, Q., Zhang, S., Wang, P., Li, Z., Qiu, Y., Yan, K., Waterhouse, G.I.N., Wang, P., Li, J., et al. (2023). Cu-C(O) interfaces deliver remarkable selectivity and stability for CO_2 reduction to C_{2+} products at industrial current density of 500 mA cm^{-2}. Small *19*, e2301289. https://doi.org/10.1002/smll.202301289.
29. Dattila, F., Garcia-Muelas, R., and López, N. (2020). Active and elective ensembles in oxide-derived copper catalysts for CO_2 reduction. ACS Energy Lett. *5*, 3176–3184. https://doi.org/10.1021/acsenergylett.0c01777.
30. Mohamed, A.G.A., Zhou, E., Zeng, Z., Xie, J., Gao, D., and Wang, Y. (2021). Asymmetric oxo-bridged ZnPb bimetallic electrocatalysis boosting CO_2-to-HCOOH reduction. Adv. Sci. *9*, e2104138. https://doi.org/10.1002/advs.202104138.
31. Sang, J., Wei, P., Liu, T., Lv, H., Ni, X., Gao, D., Zhang, J., Li, H., Zang, Y., Yang, F., et al. (2022). A reconstructed $Cu_2P_2O_7$ catalyst for selective CO_2 electroreduction to multicarbon products. Angew. Chem. Int. Ed. *61*, e202114238. https://doi.org/10.1002/anie.202114238.
32. Chen, J., and Wang, L. (2022). Effects of the catalyst dynamic changes and influence of the reaction environment on the performance of electrochemical CO_2 reduction. Adv. Mater. *34*, e2103900. https://doi.org/10.1002/adma.202103900.
33. Wang, W., Duan, J., Liu, Y., and Zhai, T. (2022). Structural reconstruction of catalysts in electroreduction reaction: identifying, understanding, and manipulating. Adv. Mater. *34*, e2110699. https://doi.org/10.1002/adma.202110699.
34. Lai, W., Ma, Z., Zhang, J., Yuan, Y., Qiao, Y., and Huang, H. (2022). Dynamic evolution of active sites in electrocatalytic CO_2 reduction reaction: fundamental understanding and recent progress. Adv. Funct. Mater. *32*, 2111193. https://doi.org/10.1002/adfm.202111193.
35. Wang, J., Tan, H.Y., Zhu, Y., Chu, H., and Chen, H.M. (2021). Linking the dynamic chemical state of catalysts with the product profile of electrocatalytic CO_2 reduction. Angew. Chem. Int. Ed. *60*, 17254–17267. https://doi.org/10.1002/anie.202017181.
36. Zou, Y., and Wang, S. (2021). An investigation of active sites for electrochemical CO_2 reduction reactions: from in situ characterization to rational design. Adv. Sci. *8*, 2003579. https://doi.org/10.1002/advs.202003579.
37. Zhang, X., Zhang, Z., Li, H., Gao, R., Xiao, M., Zhu, J., Feng, M., and Chen, Z. (2022). Insight into heterogeneous electrocatalyst design understanding for the reduction of carbon dioxide. Adv. Energy Mater. *12*, 2201461. https://doi.org/10.1002/aenm.202201461.
38. Zhang, Y., Liu, H., Zhao, S., Xie, C., Huang, Z., and Wang, S. (2023). Insights into the dynamic evolution of defects in electrocatalysts. Adv. Mater. *35*, e2209680. https://doi.org/10.1002/adma.202209680.
39. Zhou, M., Li, C., and Fang, J. (2020). Noble-metal based random alloy and intermetallic nanocrystals: syntheses and applications. Chem. Rev. *121*, 736–795. https://doi.org/10.1021/acs.chemrev.0c00436.
40. Yan, Y., Du, J.S., Gilroy, K.D., Yang, D., Xia, Y., and Zhang, H. (2017). I Intermetallic nanocrystals: syntheses and catalytic applications. Adv. Mater. *29*, 1605997. https://doi.org/10.1002/adma.201605997.
41. Wang, Y., He, J., Liu, C., Chong, W.H., and Chen, H. (2014). Thermodynamics versus kinetics in nanosynthesis. Angew. Chem. Int. Ed. *54*, 2022–2051. https://doi.org/10.1002/anie.201402986.
42. Huang, L., Liu, M., Lin, H., Xu, Y., Wu, J., Dravid, V.P., Wolverton, C., and Mirkin, C.A. (2019). Shape regulation of high-index facet nanoparticles by dealloying. Science *365*, 1159–1163. https://doi.org/10.1126/science.aax5843.
43. Xia, Y., Xia, X., and Peng, H.-C. (2015). Shape-controlled synthesis of colloidal metal nanocrystals: thermodynamic versus kinetic products. J. Am. Chem. Soc. *137*,

7947–7966. https://doi.org/10.1021/jacs.5b04641.
44. Wang, H., Zhou, S., Gilroy, K.D., Cai, Z., and Xia, Y. (2017). Icosahedral nanocrystals of noble metals: synthesis and applications. Nano Today *15*, 121–144. https://doi.org/10.1016/j.nantod.2017.06.011.
45. Zhou, S., Zhao, M., Yang, T.-H., and Xia, Y. (2019). Decahedral nanocrystals of noble metals: synthesis, characterization, and applications. Mater. Today *22*, 108–131. https://doi.org/10.1016/j.mattod.2018.04.003.
46. Li, F., Medvedeva, X.V., Medvedev, J.J., Khairullina, E., Engelhardt, H., Chandrasekar, S., Guo, Y., Jin, J., Lee, A., Thérien-Aubin, H., et al. (2021). Interplay of electrochemical and electrical effects induces structural transformations in electrocatalysts. Nat. Catal. *4*, 479–487. https://doi.org/10.1038/s41929-021-00624-y.
47. Zhang, W., Yang, Y., Tang, Y., and Gao, Q. (2022). In-situ reconstruction of catalysts in cathodic electrocatalysis: New insights into active-site structures and working mechanisms. J. Energy Chem. *70*, 414–436. https://doi.org/10.1016/j.jechem.2022.02.036.
48. Lai, W., Qiao, Y., Wang, Y., and Huang, H. (2023). Stability issues in electrochemical CO_2 reduction: recent advances in fundamental understanding and design strategies. Adv. Mater. *35*, 2306288. https://doi.org/10.1002/adma.202306288.
49. Liu, L., and Corma, A. (2021). Structural transformations of solid electrocatalysts and photocatalysts. Nat. Rev. Chem. *5*, 256–276. https://doi.org/10.1038/s41570-021-00255-8.
50. Yang, Y., Gao, P., Li, L., Pan, X., Tappertzhofen, S., Choi, S., Waser, R., Valov, I., and Lu, W.D. (2014). Electrochemical dynamics of nanoscale metallic inclusions in dielectrics. Nat. Commun. *5*, 4232. https://doi.org/10.1038/ncomms5232.
51. Deng, B., Huang, M., Zhao, X., Mou, S., and Dong, F. (2021). Interfacial electrolyte effects on electrocatalytic CO_2 reduction. ACS Catal *12*, 331–362. https://doi.org/10.1021/acscatal.1c03501.
52. Ovalle, V.J., and Waegele, M.M. (2020). Impact of electrolyte anions on the adsorption of CO on Cu electrodes. J. Phys. Chem. C *124*, 14713–14721. https://doi.org/10.1021/acs.jpcc.0c04037.
53. Zhao, Y., Zu, X., Chen, R., Li, X., Jiang, Y., Wang, Z., Wang, S., Wu, Y., Sun, Y., and Xie, Y. (2022). Industrial-current-density CO_2-to-C_{2+} electroreduction by anti-swelling anion-exchange ionomer-modified oxide-derived Cu nanosheets. J. Am. Chem. Soc. *144*, 10446–10454. https://doi.org/10.1021/jacs.2c02594.
54. Ma, M., Clark, E.L., Therkildsen, K.T., Dalsgaard, S., Chorkendorff, I., and Seger, B. (2020). Insights into the carbon balance for CO_2 electroreduction on Cu using gas diffusion electrode reactor designs. Energy Environ. Sci. *13*, 977–985. https://doi.org/10.1039/d0ee00047g.
55. Li, J., Wang, Z., McCallum, C., Xu, Y., Li, F., Wang, Y., Gabardo, C.M., Dinh, C.-T., Zhuang, T.-T., Wang, L., et al. (2019). Constraining CO coverage on copper promotes high-efficiency ethylene electroproduction. Nat. Catal. *2*, 1124–1131. https://doi.org/10.1038/s41929-019-0380-x.
56. Casebolt, R., Kimura, K.W., Levine, K., Cimada DaSilva, J.A., Kim, J., Dunbar, T.A., Suntivich, J., and Hanrath, T. (2021). Effect of electrolyte composition and concentration on pulsed potential electrochemical CO_2 reduction. ChemElectroChem *8*, 681–688. https://doi.org/10.1002/celc.202001445.
57. Tan, X., Yu, C., Song, X., Ni, L., Xu, H., Xie, Y., Wang, Z., Cui, S., Ren, Y., Li, W., et al. (2022). Robust O-Pd-Cl catalyst-electrolyte interfaces enhance CO tolerance of Pd/C catalyst for stable CO_2 electroreduction. Nano Energy *104*, 107957. https://doi.org/10.1016/j.nanoen.2022.107957.
58. Yuan, T., Wang, T., Zhang, G., Deng, W., Cheng, D., Gao, H., Zhao, J., Yu, J., Zhang, P., and Gong, J. (2022). The effect of specific adsorption of halide ions on electrochemical CO_2 reduction. Chem. Sci. *13*, 8117–8123. https://doi.org/10.1039/d2sc02689a.
59. Han, Z., Han, D., Chen, Z., Gao, J., Jiang, G., Wang, X., Lyu, S., Guo, Y., Geng, C., Yin, L., et al. (2022). Steering surface reconstruction of copper with electrolyte additives for CO_2 electroreduction. Nat. Commun. *13*, 3158. https://doi.org/10.1038/s41467-022-30819-1.
60. Kim, Y.G., Baricuatro, J.H., Javier, A., Gregoire, J.M., and Soriaga, M.P. (2014). The evolution of the polycrystalline copper surface, first to Cu(111) and then to Cu(100), at a fixed CO_2RR potential: a study by operando EC-STM. LangmuirLangmuir *30*, 15053–15056. https://doi.org/10.1021/la504445g.
61. Cheng, D., Wei, Z., Zhang, Z., Broekmann, P., Alexandrova, A.N., and Sautet, P. (2023). Restructuring and activation of Cu(111) under electrocatalytic reduction conditions. Angew. Chem. Int. Ed. *62*, e202218575. https://doi.org/10.1002/anie.202218575.
62. Ma, Z., Tsounis, C., Toe, C.Y., Kumar, P.V., Subhash, B., Xi, S., Yang, H.Y., Zhou, S., Lin, Z., Wu, K.-H., et al. (2022). Reconstructing Cu nanoparticle supported on vertical graphene surfaces via electrochemical treatment to tune the selectivity of CO_2 reduction toward valuable products. ACS Catal. *12*, 4792–4805. https://doi.org/10.1021/acscatal.1c05431.
63. Kwon, S., Kim, Y.-G., Baricuatro, J.H., and Goddard, W.A. (2021). Dramatic change in the step edges of the Cu(100) electrocatalyst upon exposure to CO: Operando observations by electrochemical STM and explanation using quantum mechanical calculations. ACS Catal. *11*, 12068–12074. https://doi.org/10.1021/acscatal.1c02844.
64. Grosse, P., Yoon, A., Rettenmaier, C., Herzog, A., Chee, S.W., and Roldan Cuenya, B. (2021). Dynamic transformation of cubic copper catalysts during CO_2 electroreduction and its impact on catalytic selectivity. Nat. Commun. *12*, 6736. https://doi.org/10.1038/s41467-021-26743-5.
65. Huang, J., Hörmann, N., Oveisi, E., Loiudice, A., De Gregorio, G.L., Andreussi, O., Marzari, N., and Buonsanti, R. (2018). Potential-induced nanoclustering of metallic catalysts during electrochemical CO_2 reduction. Nat. Commun. *9*, 3117. https://doi.org/10.1038/s41467-018-05544-3.
66. Lee, S.H., Lin, J.C., Farmand, M., Landers, A.T., Feaster, J.T., Avilés Acosta, J.E., Beeman, J.W., Ye, Y., Yano, J., Mehta, A., et al. (2021). Oxidation state and surface reconstruction of Cu under CO_2 reduction conditions from in situ X-ray characterization. J. Am. Chem. Soc. *143*, 588–592. https://doi.org/10.1021/jacs.0c10017.
67. He, C., Duan, D., Low, J., Bai, Y., Jiang, Y., Wang, X., Chen, S., Long, R., Song, L., and Xiong, Y. (2021). $Cu_{2-x}S$ derived copper nanoparticles: A platform for unraveling the role of surface reconstruction in efficient electrocatalytic CO_2-to-C_2H_4 conversion. Nano Res. *16*, 4494–4498. https://doi.org/10.1007/s12274-021-3532-7.
68. Cheng, D., Zhao, Z.J., Zhang, G., Yang, P., Li, L., Gao, H., Liu, S., Chang, X., Chen, S., Wang, T., et al. (2021). The nature of active sites for carbon dioxide electroreduction over oxide-derived copper catalysts. Nat. Commun. *12*, 395. https://doi.org/10.1038/s41467-020-20615-0.
69. Gunathunge, C.M., Ovalle, V.J., Li, Y., Janik, M.J., and Waegele, M.M. (2018). Existence of an electrochemically inert CO population on Cu electrodes in alkaline pH. ACS Catal. *8*, 7507–7516. https://doi.org/10.1021/acscatal.8b01552.
70. Zeng, D., Li, C., Wang, W., Zhang, L., Zhang, Y., Wang, J., Zhang, L., Zhou, X., and Wang, W. (2023). Insights into the hydrophobic surface promoting electrochemical CO_2 reduction to ethylene. Chem. Eng. J. *461*, 142133. https://doi.org/10.1016/j.cej.2023.142133.
71. Deng, B., Huang, M., Li, K., Zhao, X., Geng, Q., Chen, S., Xie, H., Dong, X., Wang, H., and Dong, F. (2022). The crystal plane is not the key factor for CO_2-to-methane electrosynthesis on reconstructed Cu_2O microparticles. Angew. Chem. Int. Ed. *61*, e202114080. https://doi.org/10.1002/anie.202114080.
72. Xiao, H., Goddard, W.A., 3rd, Cheng, T., and Liu, Y. (2017). Cu metal embedded in oxidized matrix catalyst to promote CO_2 activation and CO dimerization for electrochemical reduction of CO_2. Proc. Natl. Acad. Sci. USA *114*, 6685–6688. https://doi.org/10.1073/pnas.1702405114.
73. Zhang, J., Wang, Y., Li, Z., Xia, S., Cai, R., Ma, L., Zhang, T., Ackley, J., Yang, S., Wu, Y., and Wu, J. (2022). Grain boundary-derived Cu^+/Cu^0 interfaces in CuO nanosheets for low overpotential carbon dioxide electroreduction to ethylene. Adv. Sci. *9*, e2200454. https://doi.org/10.1002/advs.202200454.
74. Kim, T., and Palmore, G.T.R. (2020). A scalable method for preparing Cu electrocatalysts that convert CO_2 into C_{2+} products. Nat. Commun. *11*, 3622. https://doi.org/10.1038/s41467-020-16998-9.
75. Fu, Y., Xie, Q., Wu, L., and Luo, J. (2022). Crystal facet effect induced by different pretreatment of Cu_2O nanowire electrode for enhanced electrochemical CO_2 reduction to C_{2+} products. Chin. J. Catal. *43*, 1066–1073. https://doi.org/10.1016/s1872-2067(21)63981-5.
76. Zhao, Y., Tan, X., Yang, W., Jia, C., Chen, X., Ren, W., Smith, S.C., and Zhao, C. (2020). Surface reconstruction of ultrathin palladium nanosheets during electrocatalytic CO_2 reduction. Angew. Chem. Int. Ed. *59*, 21493–21498. https://doi.org/10.1002/anie.202009616.
77. Gao, D., Zhou, H., Cai, F., Wang, D., Hu, Y., Jiang, B., Cai, W.-B., Chen, X., Si, R., Yang, F., et al. (2017). Switchable CO_2 electroreduction via engineering active

phases of Pd nanoparticles. Nano Res. *10*, 2181–2191. https://doi.org/10.1007/s12274-017-1514-6.

78. Abdellah, A.M., Ismail, F., Siig, O.W., Yang, J., Andrei, C.M., DiCecco, L.A., Rakhsha, A., Salem, K.E., Grandfield, K., Bassim, N., et al. (2024). Impact of palladium/palladium hydride conversion on electrochemical CO_2 reduction via in-situ transmission electron microscopy and diffraction. Nat. Commun. *15*, 938. https://doi.org/10.1038/s41467-024-45096-3.
79. Li, S., Dong, X., Mao, J., Chen, W., Chen, A., Wu, G., Zhu, C., Li, G., Wei, Y., Liu, X., et al. (2023). Highly efficient CO_2 reduction at steady 2 A cm^{-2} by surface reconstruction of silver penetration electrode. Small *19*, e2301338. https://doi.org/10.1002/smll.202301338.
80. Yuan, Y., Wang, Q., Qiao, Y., Chen, X., Yang, Z., Lai, W., Chen, T., Zhang, G., Duan, H., Liu, M., and Huang, H. (2022). In situ structural reconstruction to renerate the active sites for CO_2 electroreduction on bismuth ultrathin nanosheets. Adv. Energy Mater. *12*, 2200970. https://doi.org/10.1002/aenm.202200970.
81. Yang, S., Jiang, M., Zhang, W., Hu, Y., Liang, J., Wang, Y., Tie, Z., and Jin, Z. (2023). In situ structure refactoring of bismuth nanoflowers for highly selective electrochemical reduction of CO_2 to formate. Adv. Funct. Mater. *33*, 2301984. https://doi.org/10.1002/adfm.202301984.
82. Cheng, W., Xu, X., Liao, Q., Yao, G., Zhang, C., and Li, H. (2024). In situ dynamic re-structuring and interfacial evolution of SnS_2 for high-performance electrochemical CO_2 reduction to formate. Chem. Eng. J. *480*, 147922. https://doi.org/10.1016/j.cej.2023.147922.
83. Wulan, B., Cao, X., Tan, D., Ma, J., and Zhang, J. (2022). To stabilize oxygen on In/In_2O_3 heterostructure via Joule heating for efficient electrocatalytic CO_2 reduction. Adv. Funct. Mater. *33*, 2209114. https://doi.org/10.1002/adfm.202209114.
84. Chen, Z., Zhang, D., Li, Q., Zhang, H., Zhao, Y., Ke, Q., Yan, Y., Liu, L., Liu, M., and He, X. (2024). In-situ reconstruction of $Bi_{60}In_2O_{93}$ nanotube for stable electroreduction of CO_2 at ampere-current densities. Appl. Catal. B Environ. *341*, 123342. https://doi.org/10.1016/j.apcatb.2023.123342.
85. Luo, W., Zhang, Q., Zhang, J., Moioli, E., Zhao, K., and Züttel, A. (2020). Electrochemical reconstruction of ZnO for selective reduction of CO_2 to CO. Appl. Catal. B Environ. *273*, 119060. https://doi.org/10.1016/j.apcatb.2020.119060.
86. Zhang, J., My Pham, T.H., Gao, Z., Li, M., Ko, Y., Lombardo, L., Zhao, W., Luo, W., and Züttel, A. (2023). Electrochemical CO_2 reduction over copper phthalocyanine derived catalysts with enhanced selectivity for multicarbon products. ACS Catal. *13*, 9326–9335. https://doi.org/10.1021/acscatal.3c01439.
87. Li, S.H., Hu, S., Liu, H., Liu, J., Kang, X., Ge, S., Zhang, Z., Yu, Q., and Liu, B. (2023). Two-dimensional metal coordination polymer derived indium nanosheet for efficient carbon dioxide reduction to formate. ACS Nano *17*, 9338–9346. https://doi.org/10.1021/acsnano.3c01059.
88. Liu, C., Zhang, X.-D., Huang, J.-M., Guan, M.-X., Xu, M., and Gu, Z.-Y. (2022). In Situ reconstruction of Cu–N coordinated MOFs to generate dispersive Cu/Cu_2O nanoclusters for selective electroreduction of CO_2 to C_2H_4. ACS Catal. *12*, 15230–15240. https://doi.org/10.1021/acscatal.2c04275.
89. Lamagni, P., Miola, M., Catalano, J., Hvid, M.S., Mamakhel, M.A.H., Christensen, M., Madsen, M.R., Jeppesen, H.S., Hu, X.M., Daasbjerg, K., et al. (2020). Restructuring metal–organic frameworks to nanoscale bismuth electrocatalysts for highly active and selective CO_2 reduction to formate. Adv. Funct. Mater. *30*, 1910408. https://doi.org/10.1002/adfm.201910408.
90. Yao, D., Tang, C., Vasileff, A., Zhi, X., Jiao, Y., and Qiao, S.Z. (2021). The controllable reconstruction of Bi-MOFs for electrochemical CO_2 reduction through electrolyte and potential mediation. Angew. Chem. Int. Ed. *60*, 18178–18184. https://doi.org/10.1002/anie.202104747.
91. Singh, A., Barman, S., Rahimi, F.A., Dey, A., Jena, R., Kumar, R., Mathew, N., Bhattacharyya, D., and Maji, T.K. (2024). Atomically dispersed Co^{2+} in a redox-active COF for electrochemical CO_2 reduction to ethanol: unravelling mechanistic insight through operando studies. Energy Environ. Sci. *17*, 2315–2325. https://doi.org/10.1039/d3ee02946h.
92. Xu, H., Rebollar, D., He, H., Chong, L., Liu, Y., Liu, C., Sun, C.-J., Li, T., Muntean, J.V., Winans, R.E., et al. (2020). Highly selective electrocatalytic CO_2 reduction to ethanol by metallic clusters dynamically formed from atomically dispersed copper. Nat. Energy *5*, 623–632. https://doi.org/10.1038/s41560-020-0666-x.
93. Xu, J., Patel, P., Liu, D.-J., Xu, T., and Liu, C. (2023). Understanding the dynamic evolution of atomically dispersed Cu catalyst for CO_2 electrochemical conversion using integrated XANES analysis and mechanistic studies. J. Catal. *425*, 296–305. https://doi.org/10.1016/j.jcat.2023.06.020.
94. Jang, J., Lee, K., Shin, H., Lee, H.S., Lee, B.-H., Jeong, J., Kim, J., Hwang, W., Park, S., Bootharaju, M.S., et al. (2023). Distinct reconstruction of aluminum-doped oxide-derived copper enhances the selectivity of C_{2+} products in CO_2 electroreduction. J. Mater. Chem. A *11*, 19066–19073. https://doi.org/10.1039/d3ta02375c.
95. Jia, Y., Ding, Y., Song, T., Xu, Y., Li, Y., Duan, L., Li, F., Sun, L., and Fan, K. (2023). Dynamic surface reconstruction of amphoteric metal (Zn, Al) doped Cu_2O for efficient electrochemical CO_2 reduction to C_{2+} products. Adv. Sci. *10*, e2303726. https://doi.org/10.1002/advs.202303726.
96. Feng, J., Li, J., Qiao, L., Liu, D., Zhou, P., Ni, J., and Pan, H. (2023). Reconstructed anti-poisoning surface for enhanced electrochemical CO_2 reduction on Cu-incorporated ZnO. Appl. Catal. B Environ. *330*, 122665. https://doi.org/10.1016/j.apcatb.2023.122665.
97. Niu, W., Chen, Z., Guo, W., Mao, W., Liu, Y., Guo, Y., Chen, J., Huang, R., Kang, L., Ma, Y., et al. (2023). Pb-rich Cu grain boundary sites for selective CO-to-n-propanol electroconversion. Nat. Commun. *14*, 4882. https://doi.org/10.1038/s41467-023-40689-w.
98. Chang, C.J., Lin, S.C., Chen, H.C., Wang, J., Zheng, K.J., Zhu, Y., and Chen, H.M. (2020). Dynamic reoxidation/reduction-driven atomic interdiffusion for highly selective CO_2 reduction toward methane. J. Am. Chem. Soc. *142*, 12119–12132. https://doi.org/10.1021/jacs.0c01859.
99. Zhu, C., Zhou, L., Zhang, Z., Yang, C., Shi, G., Zhao, S., Gu, H., Wu, J., Gao, X., Li, Y., et al. (2022). Dynamic restructuring of epitaxial Au–Cu biphasic interface for tandem CO_2-to-C_{2+} alcohol conversion. Chem *8*, 3288–3301. https://doi.org/10.1016/j.chempr.2022.08.016.
100. Arenas Esteban, D., Pacquets, L., Choukroun, D., Hoekx, S., Kadu, A.A., Schalck, J., Daems, N., Breugelmans, T., and Bals, S. (2023). 3D characterization of the structural transformation undergone by Cu@Ag core–shell nanoparticles following CO_2 reduction reaction. Chem. Mater. *35*, 6682–6691. https://doi.org/10.1021/acs.chemmater.3c00649.
101. Wang, H., Zhou, X., Yu, T., Lu, X., Qian, L., Liu, P., and Lei, P. (2022). Surface restructuring in AgCu single-atom alloy catalyst and self-enhanced selectivity toward CO_2 reduction. Electrochim. Acta *426*, 140774. https://doi.org/10.1016/j.electacta.2022.140774.
102. Chen, P.C., Chen, C., Yang, Y., Maulana, A.L., Jin, J., Feijoo, J., and Yang, P. (2023). Chemical and Structural Evolution of AgCu Catalysts in Electrochemical CO(2) Reduction. J. Am. Chem. Soc. *145*, 10116–10125. https://doi.org/10.1021/jacs.3c00467.
103. Wang, T., Chen, J., Ren, X., Zhang, J., Ding, J., Liu, Y., Lim, K.H., Wang, J., Li, X., Yang, H., et al. (2023). Halogen-incorporated Sn catalysts for selective electrochemical CO_2 reduction to formate. Angew. Chem. Int. Ed. *62*, e202211174. https://doi.org/10.1002/anie.202211174.
104. Lv, L., Lu, R., Zhu, J., Yu, R., Zhang, W., Cui, E., Chen, X., Dai, Y., Cui, L., Li, J., et al. (2023). Coordinating the edge defects of bismuth with sulfur for enhanced CO_2 electroreduction to formate. Angew. Chem. Int. Ed. *62*, e202303117. https://doi.org/10.1002/anie.202303117.
105. Woldu, A.R., Talebi, P., Yohannes, A.G., Xu, J., Wu, X.D., Siahrostami, S., Hu, L., and Huang, X.C. (2023). Insights into electrochemical CO_2 reduction on SnS_2: main product switch from hydrogen to formate by pulsed potential electrolysis. Angew. Chem. Int. Ed. *62*, e202301621. https://doi.org/10.1002/anie.202301621.
106. Han, J., Long, C., Zhang, J., Hou, K., Yuan, Y., Wang, D., Zhang, X., Qiu, X., Zhu, Y., Zhang, Y., et al. (2020). A reconstructed porous copper surface promotes selectivity and efficiency toward C_2 products by electrocatalytic CO_2 reduction. Chem. Sci. *11*, 10698–10704. https://doi.org/10.1039/d0sc01202e.
107. Ma, W., Xie, S., Liu, T., Fan, Q., Ye, J., Sun, F., Jiang, Z., Zhang, Q., Cheng, J., and Wang, Y. (2020). Electrocatalytic reduction of CO_2 to ethylene and ethanol through hydrogen-assisted C–C coupling over fluorine-modified copper. Nat. Catal. *3*, 478–487. https://doi.org/10.1038/s41929-020-0450-0.
108. Shi, Y., Wang, Y., Dong, C.L., Nga, T.T.T., Wei, D., Wang, J., Zhao, X., Wang, M., Zhang, K., Li, M., et al. (2023). Localized geometry determined selectivity of iodide-derived copper for electrochemical CO_2 reduction. Adv. Energy Mater. *13*, 2203896. https://doi.org/10.1002/aenm.202203896.
109. Yoon, A., Poon, J., Grosse, P., Chee, S.W., and Cuenya, B.R. (2022). Iodide-mediated Cu catalyst restructuring during CO_2

electroreduction. J. Mater. Chem. A *10*, 14041–14050. https://doi.org/10.1039/d1ta11089f.

110. Zheng, M., Wang, P., Zhi, X., Yang, K., Jiao, Y., Duan, J., Zheng, Y., and Qiao, S.-Z. (2022). Electrocatalytic CO_2-to-C_{2+} with ampere-level current on heteroatom-engineered copper via tuning *CO intermediate coverage. J. Am. Chem. Soc. *144*, 14936–14944. https://doi.org/10.1021/jacs.2c06820.
111. Liang, S., Xiao, J., Zhang, T., Zheng, Y., Wang, Q., and Liu, B. (2023). Sulfur changes the electrochemical CO_2 reduction pathway over Cu electrocatalysts. Angew. Chem. Int. Ed. *62*, e202310740. https://doi.org/10.1002/anie.202310740.
112. Wang, T., Chen, J., Ren, X., Zhang, J., Ding, J., Liu, Y., Lim, K.H., Wang, J., Li, X., Yang, H., et al. (2023). Halogen-incorporated Sn catalysts for selective electrochemical CO_2 reduction to formate. Angew. Chem. Int. Ed. *62*, e202211174. https://doi.org/10.1002/anie.202211174.
113. Gao, D., Scholten, F., and Roldan Cuenya, B. (2017). Improved CO_2 electroreduction performance on plasma-activated Cu catalysts via electrolyte design: halide effect. ACS Catal. *7*, 5112–5120. https://doi.org/10.1021/acscatal.7b01416.
114. Huang, Y., Ong, C.W., and Yeo, B.S. (2018). Effects of electrolyte anions on the reduction of carbon dioxide to ethylene and ethanol on copper (100) and (111) surfaces. ChemSusChem *11*, 3299–3306. https://doi.org/10.1002/cssc.201801078.
115. Gao, D., McCrum, I.T., Deo, S., Choi, Y.-W., Scholten, F., Wan, W., Chen, J.G., Janik, M.J., and Roldan Cuenya, B. (2018). Activity and selectivity control in CO_2 electroreduction to multicarbon products over CuO_x catalysts via electrolyte design. ACS Catal. *8*, 10012–10020. https://doi.org/10.1021/acscatal.8b02587.
116. Garg, S., Li, M., Wu, Y., Nazmi Idros, M., Wang, H., Yago, A.J., Ge, L., Wang, G.G.X., and Rufford, T.E. (2021). Understanding the effects of anion interactions with Ag electrodes on electrochemical CO_2 reduction in choline halide electrolytes. ChemSusChem *14*, 2601–2611. https://doi.org/10.1002/cssc.202100848.
117. Henckel, D.A., Counihan, M.J., Holmes, H.E., Chen, X., Nwabara, U.O., Verma, S., Rodríguez-López, J., Kenis, P.J.A., and Gewirth, A.A. (2020). Potential dependence of the local pH in a CO_2 reduction electrolyzer. ACS Catal. *11*, 255–263. https://doi.org/10.1021/acscatal.0c04297.
118. Kim, J.Y.'., Sellers, C., Hao, S., Senftle, T.P., and Wang, H. (2023). Different distributions of multi-carbon products in CO_2 and CO electroreduction under practical reaction conditions. Nat. Catal. *6*, 1115–1124. https://doi.org/10.1038/s41929-023-01082-4.
119. Li, J., Chang, X., Zhang, H., Malkani, A.S., Cheng, M.J., Xu, B., and Lu, Q. (2021). Electrokinetic and in situ spectroscopic investigations of CO electrochemical reduction on copper. Nat. Commun. *12*, 3264. https://doi.org/10.1038/s41467-021-23582-2.
120. Ovalle, V.J., and Waegele, M.M. (2021). Influence of pH and proton donor/acceptor identity on electrocatalysis in aqueous media. J. Phys. Chem. C *125*, 18567–18578. https://doi.org/10.1021/acs.jpcc.1c05921.
121. Jiang, Y., Wang, X., Duan, D., He, C., Ma, J., Zhang, W., Liu, H., Long, R., Li, Z., Kong, T., et al. (2022). Structural reconstruction of Cu_2O superparticles toward electrocatalytic CO_2 reduction with high C_{2+} products selectivity. Adv. Sci. *9*, e2105292. https://doi.org/10.1002/advs.202105292.
122. Liu, H., Yan, T., Tan, S., Sun, L., Zhang, Z., Hu, S., Li, S.H., Kang, X., Lei, Y., Jiang, L., et al. (2024). Observation on microenvironment changes of dynamic catalysts in acidic CO_2 reduction. J. Am. Chem. Soc. *146*, 5333–5342. https://doi.org/10.1021/jacs.3c12321.
123. Tao, Z., Wu, Z., Wu, Y., and Wang, H. (2020). Activating copper for electrocatalytic CO_2 reduction to formate via molecular interactions. ACS Catal. *10*, 9271–9275. https://doi.org/10.1021/acscatal.0c02237.
124. Ma, Y., Wang, J., Yu, J., Zhou, J., Zhou, X., Li, H., He, Z., Long, H., Wang, Y., Lu, P., et al. (2021). Surface modification of metal materials for high-performance electrocatalytic carbon dioxide reduction. Matter *4*, 888–926. https://doi.org/10.1016/j.matt.2021.01.007.
125. Pankhurst, J.R., Iyengar, P., Okatenko, V., and Buonsanti, R. (2021). Copper nanocrystal morphology determines the viability of molecular surface functionalization in tuning electrocatalytic behavior in CO_2 reduction. Inorg. Chem. *60*, 6939–6945. https://doi.org/10.1021/acs.inorgchem.1c00287.
126. Cheng, Y., Hou, J., and Kang, P. (2021). Integrated capture and electroreduction of flue gas CO_2 to formate using amine functionalized SnO_x nanoparticles. ACS Energy Lett. *6*, 3352–3358. https://doi.org/10.1021/acsenergylett.1c01553.
127. Abdinejad, M., Mirza, Z., Zhang, X.-A., and Kraatz, H.-B. (2020). Enhanced electrocatalytic activity of primary amines for CO_2 reduction using copper electrodes in aqueous solution. ACS Sustain. Chem. Eng. *8*, 1715–1720. https://doi.org/10.1021/acssuschemeng.9b06837.
128. Shi, Y., Sun, K., Shan, J., Li, H., Gao, J., Chen, Z., Sun, C., Shuai, Y., and Wang, Z. (2022). Selective CO_2 electromethanation on surface-modified Cu catalyst by local microenvironment modulation. ACS Catal. *12*, 8252–8258. https://doi.org/10.1021/acscatal.2c01544.
129. Iijima, G., Yamaguchi, H., Inomata, T., Yoto, H., Ito, M., and Masuda, H. (2020). Methanethiol SAMs induce reconstruction and formation of Cu^+ on a Cu catalyst under electrochemical CO_2 reduction. ACS Catal. *10*, 15238–15249. https://doi.org/10.1021/acscatal.0c04106.
130. Pan, H., Wang, F., She, S., Zhang, Z., and Min, S. (2023). Boosting CO_2 electroreduction on a Zn electrode via concurrent surface reconstruction and interfacial surfactant modification. Dalton Trans. *52*, 556–561. https://doi.org/10.1039/d2dt03685a.
131. Kang, C., Li, Y., Xu, Y., Ding, C., Chen, H., Zeng, J., Li, Y., Li, C., and He, J. (2023). Coupling CO_2-to-ethylene reduction with the chlor-alkaline process in seawater through in situ-formed Cu catalysts. J. Phys. Chem. Lett. *14*, 2983–2989. https://doi.org/10.1021/acs.jpclett.3c00179.
132. Ge, W., Chen, Y., Fan, Y., Zhu, Y., Liu, H., Song, L., Liu, Z., Lian, C., Jiang, H., and Li, C. (2022). Dynamically formed surfactant assembly at the electrified electrode-electrolyte interface boosting CO_2 electroreduction. J. Am. Chem. Soc. *144*, 6613–6622. https://doi.org/10.1021/jacs.2c02486.
133. Casebolt, R., Levine, K., Suntivich, J., and Hanrath, T. (2021). Pulse check: Potential opportunities in pulsed electrochemical CO_2 reduction. Joule *5*, 1987–2026. https://doi.org/10.1016/j.joule.2021.05.014.
134. Obasanjo, C.A., Gao, G., Khiarak, B.N., Pham, T.H., Crane, J., and Dinh, C.-T. (2023). Progress and perspectives of pulse electrolysis for stable electrochemical carbon dioxide reduction. Energy Fuels *37*, 13601–13623. https://doi.org/10.1021/acs.energyfuels.3c02152.
135. Xu, L., Ma, X., Wu, L., Tan, X., Song, X., Zhu, Q., Chen, C., Qian, Q., Liu, Z., Sun, X., et al. (2022). In situ periodic regeneration of catalyst during CO_2 electroreduction to C_{2+} products. Angew. Chem. Int. Ed. *61*, e202210375. https://doi.org/10.1002/anie.202210375.
136. Xu, Z., Xie, Y., and Wang, Y. (2023). Pause electrolysis for acidic CO_2 reduction on 3-dimensional Cu. Mater. Rep. Energy *3*, 100173. https://doi.org/10.1016/j.matre.2022.100173.
137. Casebolt DiDomenico, R., Levine, K., Bundschu, C., Reimanis, L., Arias, T., and Hanrath, T. (2024). Pulsing the applied potential in electrochemical CO_2 reduction enhances the C_2 activity by modulating the dynamic competitive binding of *CO and *H. ACS Catal. *14*, 785–796. https://doi.org/10.1021/acscatal.3c04224.
138. Hua, W., Liu, T., Zheng, Z., Yuan, H., Xiao, L., Feng, K., Hui, J., Deng, Z., Ma, M., Cheng, J., et al. (2024). Pulse electrolysis turns on CO_2 methanation through N-confused cupric porphyrin. Angew. Chem. Int. Ed. *63*, e202315922. https://doi.org/10.1002/anie.202315922.
139. Shiratsuchi, R., Aikoh, Y., and Nogami, G. (1993). Pulsed electroreduction of CO_2 on copper electrodes. J. Electrochem. Soc. *140*, 3479–3482.
140. Shiratsuchi, R., and Nogami, G. (1996). Pulsed electroreduction of CO_2 on silver electrodes. J. Electrochem. Soc. *143*, 582–586.
141. Ishimaru, S., Shiratsuchi, R., and Nogami, G. (2000). Pulsed electroreduction of CO_2 on Cu-Ag alloy electrodes. J. Electrochem. Soc. *147*, 1864–1867. https://doi.org/10.1149/1.1393448.
142. Lee, J., and Tak, Y. (2001). Electrocatalytic activity of Cu electrode in electroreduction of CO_2. Electrochim. Acta *46*, 3015–3022.
143. Yano, J., and Yamasaki, S. (2008). Pulse-mode electrochemical reduction of carbon dioxide using copper and copper oxide electrodes for selective ethylene formation. J. Appl. Electrochem. *38*, 1721–1726. https://doi.org/10.1007/s10800-008-9622-3.
144. Kimura, K.W., Fritz, K.E., Kim, J., Suntivich, J., Abruña, H.D., and Hanrath, T. (2018). Controlled selectivity of CO_2 reduction on copper by pulsing the electrochemical potential. ChemSusChem *11*, 1781–1786. https://doi.org/10.1002/cssc.201800318.
145. Kim, C., Weng, L.-C., and Bell, A.T. (2020). Impact of pulsed electrochemical reduction of CO_2 on the formation of C_{2+} products over Cu. ACS Catal. *10*, 12403–12413. https://doi.org/10.1021/acscatal.0c02915.
146. Kimura, K.W., Casebolt, R., Cimada DaSilva, J., Kauffman, E., Kim, J., Dunbar, T.A., Pollock, C.J., Suntivich, J., and Hanrath, T. (2020). Selective electrochemical CO_2 reduction during pulsed potential stems

from dynamic interface. ACS Catal. *10*, 8632–8639. https://doi.org/10.1021/acscatal.0c02630.

147. Bui, J.C., Kim, C., Weber, A.Z., and Bell, A.T. (2021). Dynamic boundary layer simulation of pulsed CO_2 electrolysis on a copper catalyst. ACS Energy Lett. *6*, 1181–1188. https://doi.org/10.1021/acsenergylett.1c00364.
148. Wu, X., Li, X., Lv, J., Lv, X., Wu, A., Qi, Z., and Wu, H.B. (2024). Pulsed electrolysis promotes CO_2 reduction to ethanol on heterostructured Cu_2O/Ag catalysts. Small *20*, e2307637. https://doi.org/10.1002/smll.202307637.
149. Xu, L., Feng, J., Wu, L., Song, X., Tan, X., Zhang, L., Ma, X., Jia, S., Du, J., Chen, A., et al. (2023). Identifying the optimal oxidation state of Cu for electrocatalytic reduction of CO_2 to C_{2+} products. Green Chem. *25*, 1326–1331. https://doi.org/10.1039/d2gc04368h.
150. Arán-Ais, R.M., Scholten, F., Kunze, S., Rizo, R., and Roldan Cuenya, B. (2020). The role of in situ generated morphological motifs and Cu(I) species in C_{2+} product selectivity during CO_2 pulsed electroreduction. Nat. Energy *5*, 317–325. https://doi.org/10.1038/s41560-020-0594-9.
151. Li, Z., Wang, L., Wang, T., Sun, L., and Yang, W. (2023). Steering the dynamics of reaction intermediates and catalyst surface during electrochemical pulsed CO_2 reduction for enhanced C_{2+} selectivity. J. Am. Chem. Soc. *145*, 20655–20664. https://doi.org/10.1021/jacs.3c08005.
152. Zhang, X.D., Liu, T., Liu, C., Zheng, D.S., Huang, J.M., Liu, Q.W., Yuan, W.W., Yin, Y., Huang, L.R., Xu, M., et al. (2023). Asymmetric low-frequency pulsed strategy enables ultralong CO_2 reduction stability and controllable product selectivity. J. Am. Chem. Soc. *145*, 2195–2206. https://doi.org/10.1021/jacs.2c09501.
153. Velasco-Velez, J.-J., Mom, R.V., Sandoval-Diaz, L.-E., Falling, L.J., Chuang, C.-H., Gao, D., Jones, T.E., Zhu, Q., Arrigo, R., Roldan Cuenya, B., et al. (2020). Revealing the active phase of copper during the electroreduction of CO_2 in aqueous electrolyte by correlating in situ X-ray spectroscopy and in situ electron microscopy. ACS Energy Lett. *5*, 2106–2111. https://doi.org/10.1021/acsenergylett.0c00802.
154. Grosse, P., Gao, D., Scholten, F., Sinev, I., Mistry, H., and Roldan Cuenya, B. (2018). Dynamic changes in the structure, chemical state and catalytic selectivity of Cu nanocubes during CO_2 electroreduction: size and support effects. Angew. Chem. Int. Ed. *57*, 6192–6197. https://doi.org/10.1002/anie.201802083.
155. Simon, G.H., Kley, C.S., and Roldan Cuenya, B. (2021). Potential-dependent morphology of copper catalysts during CO_2 electroreduction revealed by in situ atomic force microscopy. Angew. Chem. Int. Ed. *60*, 2561–2568. https://doi.org/10.1002/anie.202010449.
156. Munz, M., Poon, J., Frandsen, W., Cuenya, B.R., and Kley, C.S. (2023). Nanoscale electron transfer variations at electrocatalyst–electrolyte interfaces resolved by in situ conductive atomic force microscopy. J. Am. Chem. Soc. *145*, 5242–5251. https://doi.org/10.1021/jacs.2c12617.
157. Vavra, J., Shen, T.H., Stoian, D., Tileli, V., and Buonsanti, R. (2021). Real-time monitoring reveals dissolution/redeposition mechanism in copper nanocatalysts during the initial stages of the CO_2 reduction reaction. Angew. Chem. Int. Ed. *60*, 1347–1354. https://doi.org/10.1002/anie.202011137.
158. Hsu, C.-S., Wang, J., Chu, Y.-C., Chen, J.-H., Chien, C.-Y., Lin, K.-H., Tsai, L.D., Chen, H.-C., Liao, Y.-F., Hiraoka, N., et al. (2023). Activating dynamic atomic-configuration for single-site electrocatalyst in electrochemical CO_2 reduction. Nat. Commun. *14*, 5245. https://doi.org/10.1038/s41467-023-40970-y.
159. Phan, T.H., Banjac, K., Cometto, F.P., Dattila, F., García-Muelas, R., Raaijman, S.J., Ye, C., Koper, M.T.M., López, N., and Lingenfelder, M. (2021). Emergence of potential-controlled Cu-nanocuboids and graphene-covered Cu-nanocuboids under operando CO_2 electroreduction. Nano Lett. *21*, 2059–2065. https://doi.org/10.1021/acs.nanolett.0c04703.
160. Amirbeigiarab, R., Tian, J., Herzog, A., Qiu, C., Bergmann, A., Roldan Cuenya, B., and Magnussen, O.M. (2023). Atomic-scale surface restructuring of copper electrodes under CO_2 electroreduction conditions. Nat. Catal. *6*, 837–846. https://doi.org/10.1038/s41929-023-01009-z.
161. Zhu, C., Zhang, Z., Zhong, L., Hsu, C.-S., Xu, X., Li, Y., Zhao, S., Chen, S., Yu, J., Chen, S., et al. (2021). Product-specific active site motifs of Cu for electrochemical CO_2 reduction. Chem *7*, 406–420. https://doi.org/10.1016/j.chempr.2020.10.018.
162. Su, X., Jiang, Z., Zhou, J., Liu, H., Zhou, D., Shang, H., Ni, X., Peng, Z., Yang, F., Chen, W., et al. (2022). Complementary operando spectroscopy identification of in-situ generated metastable charge-asymmetry Cu_2-CuN_3 clusters for CO_2 reduction to ethanol. Nat. Commun. *13*, 1322. https://doi.org/10.1038/s41467-022-29035-8.
163. Sheng, W., Kattel, S., Yao, S., Yan, B., Liang, Z., Hawxhurst, C.J., Wu, Q., and Chen, J.G. (2017). Electrochemical reduction of CO_2 to synthesis gas with controlled CO/H_2 ratios. Energy Environ. Sci. *10*, 1180–1185. https://doi.org/10.1039/c7ee00071e.
164. Yang, S., An, H., Arnouts, S., Wang, H., Yu, X., de Ruiter, J., Bals, S., Altantzis, T., Weckhuysen, B.M., and van der Stam, W. (2023). Halide-guided active site exposure in bismuth electrocatalysts for selective CO_2 conversion into formic acid. Nat. Catal. *6*, 796–806. https://doi.org/10.1038/s41929-023-01008-0.
165. Li, S., Dong, X., Mao, J., Chen, W., Chen, A., Wu, G., Zhu, C., Li, G., Wei, Y., Liu, X., et al. (2023). Highly efficient CO_2 reduction at steady 2 A cm^{-2} by surface reconstruction of silver penetration electrode. Small *19*, 2301338. https://doi.org/10.1002/smll.202301338.
166. Choi, Y.-W., Scholten, F., Sinev, I., and Roldan Cuenya, B. (2019). Enhanced stability and CO/formate selectivity of plasma-treated SnO_x/AgO_x catalysts during CO_2 electroreduction. J. Am. Chem. Soc. *141*, 5261–5266. https://doi.org/10.1021/jacs.8b12766.
167. He, M., Li, C., Zhang, H., Chang, X., Chen, J.G., Goddard, W.A., 3rd, Cheng, M.J., Xu, B., and Lu, Q. (2020). Oxygen induced promotion of electrochemical reduction of CO_2 via co-electrolysis. Nat. Commun. *11*, 3844. https://doi.org/10.1038/s41467-020-17690-8.
168. Chang, F., Liu, Y., Wei, J., Yang, L., and Bai, Z. (2023). In situ surface/interface generation on Cu_2O nanostructures toward enhanced electrocatalytic CO_2 reduction to ethylene using operando spectroscopy. Inorg. Chem. Front. *10*, 240–249. https://doi.org/10.1039/d2qi01977a.
169. de Ruiter, J., An, H., Wu, L., Gijsberg, Z., Yang, S., Hartman, T., Weckhuysen, B.M., and van der Stam, W. (2022). Probing the dynamics of low-overpotential CO_2-to-CO activation on copper electrodes with time-resolved Raman spectroscopy. J. Am. Chem. Soc. *144*, 15047–15058. https://doi.org/10.1021/jacs.2c03172.
170. Xia, W., Xie, Y., Jia, S., Han, S., Qi, R., Chen, T., Xing, X., Yao, T., Zhou, D., Dong, X., et al. (2023). Adjacent copper single atoms promote C–C coupling in electrochemical CO_2 reduction for the efficient conversion of ethanol. J. Am. Chem. Soc. *145*, 17253–17264. https://doi.org/10.1021/jacs.3c04612.
171. Li, F., Li, Y.C., Wang, Z., Li, J., Nam, D.-H., Lum, Y., Luo, M., Wang, X., Ozden, A., Hung, S.-F., et al. (2019). Cooperative CO_2-to-ethanol conversion via enriched intermediates at molecule–metal catalyst interfaces. Nat. Catal. *3*, 75–82. https://doi.org/10.1038/s41929-019-0383-7.
172. Zhan, C., Dattila, F., Rettenmaier, C., Bergmann, A., Kühl, S., García-Muelas, R., López, N., and Cuenya, B.R. (2021). Revealing the CO coverage-driven C–C coupling mechanism for electrochemical CO_2 reduction on Cu_2O nanocubes via operando Raman spectroscopy. ACS Catal. *11*, 7694–7701. https://doi.org/10.1021/acscatal.1c01478.
173. Rettenmaier, C., Herzog, A., Casari, D., Rüscher, M., Jeon, H.S., Kordus, D., Luna, M.L., Kühl, S., Hejral, U., Davis, E.M., et al. (2024). Operando insights into correlating CO coverage and Cu–Au alloying with the selectivity of Au NP-decorated Cu_2O nanocubes during the electrocatalytic CO_2 reduction. EES Catal. *2*, 311–323. https://doi.org/10.1039/d3ey00162h.
174. Yao, K., Li, J., Wang, H., Lu, R., Yang, X., Luo, M., Wang, N., Wang, Z., Liu, C., Jing, T., et al. (2022). Mechanistic insights into OC-COH coupling in CO_2 electroreduction on fragmented copper. J. Am. Chem. Soc. *144*, 14005–14011. https://doi.org/10.1021/jacs.2c01044.
175. Wei, P., Gao, D., Liu, T., Li, H., Sang, J., Wang, C., Cai, R., Wang, G., and Bao, X. (2023). Coverage-driven selectivity switch from ethylene to acetate in high-rate CO_2/CO electrolysis. Nat. Nanotechnol. *18*, 299–306. https://doi.org/10.1038/s41565-022-01286-y.
176. Lee, S.Y., Kim, J., Bak, G., Lee, E., Kim, D., Yoo, S., Kim, J., Yun, H., and Hwang, Y.J. (2023). Probing cation effects on *CO intermediates from electroreduction of CO_2 through operando Raman spectroscopy. J. Am. Chem. Soc. *145*, 23068–23075. https://doi.org/10.1021/jacs.3c05799.
177. Li, F., Thevenon, A., Rosas-Hernández, A., Wang, Z., Li, Y., Gabardo, C.M., Ozden, A., Dinh, C.T., Li, J., Wang, Y., et al. (2020). Molecular tuning of CO_2-to-ethylene conversion. Nature *577*, 509–513. https://doi.org/10.1038/s41586-019-1782-2.
178. Xu, A., Hung, S.-F., Cao, A., Wang, Z., Karmodak, N., Huang, J.E., Yan, Y., Sedighian Rasouli, A., Ozden, A., Wu, F.-Y., et al. (2022). Copper/alkaline earth metal

oxide interfaces for electrochemical CO_2-to-alcohol conversion by selective hydrogenation. Nat. Catal. *5*, 1081–1088. https://doi.org/10.1038/s41929-022-00880-6.

179. Chen, X., Chen, J., Alghoraibi, N.M., Henckel, D.A., Zhang, R., Nwabara, U.O., Madsen, K.E., Kenis, P.J.A., Zimmerman, S.C., and Gewirth, A.A. (2020). Electrochemical CO_2-to-ethylene conversion on polyamine-incorporated Cu electrodes. Nat. Catal. *4*, 20–27. https://doi.org/10.1038/s41929-020-00547-0.
180. Lu, X., Zhu, C., Wu, Z., Xuan, J., Francisco, J.S., and Wang, H. (2020). In situ observation of the pH gradient near the gas diffusion electrode of CO_2 reduction in alkaline electrolyte. J. Am. Chem. Soc. *142*, 15438–15444. https://doi.org/10.1021/jacs.0c06779.
181. Wu, M., Huang, D., Lai, F., Yang, R., Liu, Y., Fang, J., Zhai, T., and Liu, Y. (2023). Sequential *CO management via controlling in situ reconstruction for efficient industrial-current-density CO_2-to-C_{2+} electroreduction. Proc. Natl. Acad. Sci. USA *120*, e2302851120. https://doi.org/10.1073/pnas.
182. Shan, W., Liu, R., Zhao, H., He, Z., Lai, Y., Li, S., He, G., and Liu, J. (2020). In situ surface-enhanced Raman spectroscopic evidence on the origin of selectivity in CO_2 electrocatalytic reduction. ACS Nano *14*, 11363–11372. https://doi.org/10.1021/acsnano.0c03534.
183. Shan, W., Liu, R., Zhao, H., and Liu, J. (2022). Bicarbonate rebalances the *COOH/*OCO^- dual pathways in CO_2 electrocatalytic reduction: in situ surface-enhanced Raman spectroscopic evidence. J. Phys. Chem. Lett. *13*, 7296–7305. https://doi.org/10.1021/acs.jpclett.2c01372.
184. Zhao, Y., Zhang, X.-G., Bodappa, N., Yang, W.-M., Liang, Q., Radjenovica, P.M., Wang, Y.-H., Zhang, Y.-J., Dong, J.-C., Tian, Z.-Q., and Li, J.-F. (2022). Elucidating electrochemical CO_2 reduction reaction processes on Cu(hkl) single-crystal surfaces by in situ Raman spectroscopy. Energy Environ. Sci. *15*, 3968–3977. https://doi.org/10.1039/d2ee01334g.
185. Innocent, B., Pasquier, D., Ropital, F., Hahn, F., Léger, J.M., and Kokoh, K.B. (2010). FTIR spectroscopy study of the reduction of carbon dioxide on lead electrode in aqueous medium. Appl. Catal. B Environ. *94*, 219–224. https://doi.org/10.1016/j.apcatb.2009.10.027.
186. Firet, N.J., and Smith, W.A. (2016). Probing the reaction mechanism of CO_2 electroreduction over Ag films via operando infrared spectroscopy. ACS Catal. *7*, 606–612. https://doi.org/10.1021/acscatal.6b02382.
187. Bagchi, D., Sarkar, S., Singh, A.K., Vinod, C.P., and Peter, S.C. (2022). Potential- and time-dependent dynamic nature of an oxide-derived PdIn nanocatalyst during electrochemical CO_2 reduction. ACS Nano *16*, 6185–6196. https://doi.org/10.1021/acsnano.1c11664.
188. Xue, L., Zhang, C., Shi, T., Liu, S., Zhang, H., Sun, M., Liu, F., Liu, Y., Wang, Y., Gu, X., and Zeng, S. (2023). Unraveling the improved CO_2 adsorption and COOH* formation over Cu-decorated ZnO nanosheets for CO_2 reduction toward CO. Chem. Eng. J. *452*, 139701. https://doi.org/10.1016/j.cej.2022.139701.
189. Wang, J., Huang, Y.-C., Wang, Y., Deng, H., Shi, Y., Wei, D., Li, M., Dong, C.-L., Jin, H., Mao, S.S., and Shen, S. (2023). Atomically dispersed metal–nitrogen–carbon catalysts with d-orbital electronic configuration-dependent selectivity for electrochemical CO_2-to-CO reduction. ACS Catal. *13*, 2374–2385. https://doi.org/10.1021/acscatal.2c05249.
190. Liu, H., Su, Y., Liu, Z., Chuai, H., Zhang, S., and Ma, X. (2023). Tailoring microenvironment for enhanced electrochemical CO_2 reduction on ultrathin tin oxide derived nanosheets. Nano Energy *105*, 108031. https://doi.org/10.1016/j.nanoen.2022.108031.
191. Feng, X., Zou, H., Zheng, R., Wei, W., Wang, R., Zou, W., Lim, G., Hong, J., Duan, L., and Chen, H. (2022). Bi_2O_3/BiO_2 nanoheterojunction for highly efficient electrocatalytic CO_2 reduction to formate. Nano Lett. *22*, 1656–1664. https://doi.org/10.1021/acs.nanolett.1c04683.
192. Jiang, T.-W., Qin, X., Ye, K., Zhang, W.-Y., Li, H., Liu, W., Huo, S., Zhang, X.-G., Jiang, K., and Cai, W.-B. (2023). An interactive study of catalyst and mechanism for electrochemical CO_2 reduction to formate on Pd surfaces. Appl. Catal. B Environ. *334*, 122815. https://doi.org/10.1016/j.apcatb.2023.122815.
193. Jiang, X., Wang, Q., Xiao, X., Chen, J., Shen, Y., and Wang, M. (2020). Interfacial engineering of bismuth with reduced graphene oxide hybrid for improving CO_2 electroreduction performance. Electrochim. Acta *357*, 136840. https://doi.org/10.1016/j.electacta.2020.136840.
194. Wang, X., Jiang, X., Wang, Q., Zhang, T., Li, P., Wang, M., and Shen, Y. (2020). Investigation on In–TiO_2 composites as highly efficient elecctrocatalyst for CO_2 reduction. Electrochim. Acta *340*, 135948. https://doi.org/10.1016/j.electacta.2020.135948.
195. Pan, J., Li, P., Jiang, X., Shen, Y., and Wang, M. (2023). Electrochemical CO_2 reduction on few-atomic-layer bismuth nanosheets. Mater. Today Phys. *35*, 101096. https://doi.org/10.1016/j.mtphys.2023.101096.